POLITECNICO DI TORINO
Repository ISTITUZIONALE

Measurements of inclusive jet spectra in pp and central Pb-Pb collisions at sNN =5.02 TeV

(Article begins on next page)

01 May 2024

Measurements of inclusive jet spectra in *pp* and central Pb-Pb collisions at $\sqrt{s_{NN}} = 5.02$ TeV

S. Acharya *et al.**
(ALICE Collaboration)

This article reports measurements of the p_T-differential inclusive jet cross section in *pp* collisions at $\sqrt{s} = 5.02$ TeV and the p_T-differential inclusive jet yield in Pb-Pb 0–10% central collisions at $\sqrt{s_{NN}} = 5.02$ TeV. Jets were reconstructed at midrapidity with the ALICE tracking detectors and electromagnetic calorimeter using the anti-k_T algorithm. For *pp* collisions, we report jet cross sections for jet resolution parameters $R = 0.1$–0.6 over the range $20 < p_\mathrm{T,jet} < 140$ GeV/c, as well as the jet cross-section ratios of different R and comparisons to two next-to-leading-order (NLO)–based theoretical predictions. For Pb-Pb collisions, we report the $R = 0.2$ and $R = 0.4$ jet spectra for $40 < p_\mathrm{T,jet} < 140$ GeV/c and $60 < p_\mathrm{T,jet} < 140$ GeV/c, respectively. The scaled ratio of jet yields observed in Pb-Pb to *pp* collisions, R_AA, is constructed, and exhibits strong jet quenching and a clear p_T dependence for $R = 0.2$. No significant R dependence of the jet R_AA is observed within the uncertainties of the measurement. These results are compared to several theoretical predictions.

I. INTRODUCTION

A deconfined state of strongly interacting matter described by quantum chromodynamics (QCD) is produced in ultra-relativistic heavy-ion collisions at the Relativistic Heavy Ion Collider (RHIC) and the Large Hadron Collider (LHC) [1–8]. Numerous observables including high-p_T hadron suppression, anisotropic flow, and J/ψ suppression and recombination provide evidence that the hot QCD state produced in these collisions consists of subnucleonic degrees of freedom.

One of the major strategies to investigate this hot QCD state is the study of jet modification in heavy-ion collisions. Partons often traverse a significant path length of the hot QCD medium, and the effect that the medium has on the resulting jets can be deduced by comparing jet properties in heavy-ion collisions to those in *pp* collisions. Since the jet production cross section can be computed in perturbative QCD, and since jets are sensitive to a wide range of momentum exchanges with the medium, jet physics is an appealing tool to investigate the medium at a wide range of resolution scales.

Previous measurements demonstrate suppression of the jet transverse momentum (p_T) spectrum in heavy-ion collisions relative to *pp* collisions scaled by the number of incoherent binary nucleon-nucleon collisions, indicating that jets transfer energy to the hot QCD medium [9–15]. Furthermore, jet sub-structure measurements indicate that in heavy-ion collisions, the jet core is more collimated and fragments are harder [16],

while at wide angles from the jet axis there is an excess of soft particles [17,18]. Jet modification in heavy-ion collisions is described by several different theoretical approaches typically based on energy loss via medium-induced gluon radiation and elastic scattering [19–22, and references therein]; however, there remains no clear consensus of the precise nature of the interaction of jets with the medium. New measurements of the absolute level of jet suppression and its p_T dependence will directly test models and serve as a key constraint for global analyses of high-p_T observables. Additionally, the evolution of jet suppression with the jet resolution parameter, R, can constrain competing effects between the recovery of out-of-cone radiation and the changing selection of the jet population (such as reduction of the quark/gluon fraction) as R increases [23–25].

The inclusive jet cross section in *pp* collisions contains important QCD physics itself. In recent years, the inclusive jet cross section in *pp* collisions was computed at NLO with resummation of logarithms of the jet resolution parameter [26–29] and threshold logarithms [30,31], and also to NNLO both with and without the leading color approximation [32,33]. Measurements of the inclusive *pp* jet cross section have been made at the SPS [34,35], the Tevatron [36,37], RHIC [38], and the LHC [39–47], and the latest comparisons of these measurements with theoretical predictions demonstrate the importance of contributions beyond NLO fixed-order calculations, namely resummations or matched parton showers. However, the precise contributions of the perturbative aspect of the jet, as well as the hadronization and underlying event (UE) effects, remain under investigation. Inclusive jet measurements at low-p_T as a function of R (including ratios of jet cross sections, which allow partial cancellation of experimental and theoretical uncertainties) will help clarify these contributions and provide tests for both the perturbative and nonperturbative contributions to the

---

*Full author list given at the end of the article.

inclusive jet cross section. Moreover, these measurements can be used to constrain parton distribution functions (PDFs) and the strong coupling constant α_s [43,45,48–50].

This article reports measurements of inclusive jet p_T spectra in pp and central Pb-Pb collisions at $\sqrt{s_{NN}} = 5.02$ TeV with the ALICE detector. Jets were reconstructed in the pseudorapidity range $|\eta_{\mathrm{jet}}| < 0.7 - R$ for jet resolution parameters $R = 0.1$–0.6 in pp collisions and $R = 0.2$ and $R = 0.4$ in Pb-Pb collisions. In Pb-Pb collisions, we required jets to contain at least one charged track with $p_T > 5$–7 GeV/c (depending on the jet R) in order to identify hard jet candidates (arising from large momentum-transfer scatterings) in the large background from combinatorial jets. In pp collisions, we report the cross section both with and without this bias. The relative jet yields observed in Pb-Pb and pp collisions are reported using their scaled ratio, R_{AA}, and compared to several theoretical predictions.

II. EXPERIMENTAL SETUP AND DATASETS

The ALICE detector [51,52] is a dedicated heavy-ion experiment located at the Large Hadron Collider [53]. The analysis relied on the central tracking system and the electromagnetic calorimeter (EMCal), as well as detectors for event triggering and centrality determination. The tracking system consists of a six-layer silicon inner tracking system (ITS) with radial distance 3.9–43 cm from the beamline, and a gas time projection chamber (TPC) with radial distance 85–247 cm from the beamline. The combined tracking system spans $|\eta| < 0.9$ and full azimuth, and tracks were measured in the range 150 MeV/$c < p_{T,\mathrm{track}} < 100$ GeV/c. The EMCal consists of a Pb-scintillator sampling calorimeter spanning $|\eta| < 0.7$ and $1.4 < \varphi < 3.3$ in azimuth, located a radial distance 4.36 m from the beamline [54]. It contains 12 288 cells organized in an approximately projective geometry relative to the interaction point. The Moliere radius of the EMCal is $r_M = 3.2$ cm, and its cells have a transverse size of approximately 6.0×6.0 cm ($\Delta\eta \times \Delta\varphi \approx 0.014 \times 0.014$). Each cell has a depth of 24.6 cm, corresponding to approximately 20 electromagnetic radiation lengths and one hadronic interaction length.

The reported Pb-Pb (pp) data were recorded in 2015 (2017) at $\sqrt{s_{NN}} = 5.02$ TeV. The events were collected using a minimum bias (MB) trigger requiring a coincidence hit in both of the V0 scintillators, located at $2.8 < \eta < 5.1$ (V0-A) and $-3.7 < \eta < -1.7$ (V0-C) [55]. An accepted event was required to have a primary vertex successfully reconstructed within -10 cm $< z < 10$ cm of the interaction point and to satisfy several vertex quality criteria. In Pb-Pb collisions, the centrality was determined using the V0 multiplicities [56–58]. Additionally, out-of-bunch pileup was rejected using timing cuts as well as correlating track multiplicities between several subdetectors. We utilized a sample of approximately 4.6M 0–10% most central Pb-Pb accepted events (6.0 μb^{-1}) and 760M pp accepted events (15.7 nb^{-1}).

Reconstructed tracks were generally required to include at least one hit in the silicon pixel detector (SPD) comprising the first two layers of the ITS and to have at least 70 TPC space points and at least 80% of the geometrically findable space points in the TPC. Tracks without any hits in the SPD, but otherwise satisfying the tracking criteria, were refit with a constraint to the primary vertex of the event. Including this second class of tracks ensured approximately uniform acceptance in φ, while preserving similar p_T resolution to tracks with SPD hits. Tracks with $p_{T,\mathrm{track}} > 150$ MeV/c were accepted over $-0.9 < \eta < 0.9$, $0 < \varphi < 2\pi$. The performance of the detector was estimated with a model of the ALICE detector and its response to particles using GEANT3. The tracking efficiency in pp collisions, as estimated by PYTHIA8 MONASH 2013 [59] and the ALICE GEANT3 detector simulation, is approximately 67% at $p_{T,\mathrm{track}} = 150$ MeV/c, rises to approximately 84% at $p_{T,\mathrm{track}} = 1$ GeV/c, and remains above 75% at higher p_T. Studies of the centrality dependence of the tracking efficiency in a HIJING [60] simulation demonstrated that the tracking efficiency is approximately 2% lower in 0–10% central Pb-Pb collisions compared to pp collisions, independent of $p_{T,\mathrm{track}}$. The momentum resolution $\delta p_T / p_T$ was estimated from the covariance matrix of the track fit [52] using PYTHIA8 MONASH 2013, and was approximately 1% at $p_{T,\mathrm{track}} = 1$ GeV/c and 4% at $p_{T,\mathrm{track}} = 50$ GeV/c.

Reconstructed EMCal clusters were built by clustering EMCal cells with $E_{\mathrm{cell}} > 100$ MeV around a seed cell with $E_{\mathrm{seed}} > 300$ MeV, using a clustering algorithm that allows each cluster to have only a single local maximum. The highest-energy cell in a cluster was required to satisfy a timing cut. Clusters with large apparent energy but anomalously small number of contributing cells were removed from the analysis, since they are believed to be due to interactions of slow neutrons or highly ionizing particles in the avalanche photodiodes [9]. The linearity of the energy response of the EMCal was determined from electron test beam data, and a correction of about 7% at $E_{\mathrm{cluster}} = 0.5$ GeV but negligible above $E_{\mathrm{cluster}} = 3$ GeV was applied to the cluster energies. A study using the photon conversion method demonstrated that with this nonlinearity correction, the π^0 mass in Monte Carlo (MC) simulations matches that in pp data within 1%. For pp collisions, an additional correction obtained from a photon conversion analysis was used to reduce the small remaining offset of the energy scale in data and MC simulations [61]. The energy resolution obtained from electron test beam data was about 15% at $E_{\mathrm{cluster}} = 0.5$ GeV and better than 5% above $E_{\mathrm{cluster}} = 3$ GeV.

Since the jet energy is reconstructed by combining tracks and clusters, one needs to account for the fact that charged particles deposit energy in both the tracking system and the EMCal, as in Ref. [40]. In particular, all accepted tracks were propagated to the average shower depth of the EMCal, $r = 440$ cm, and allowed to match geometrically to at most one cluster; clusters were allowed to have multiple matching tracks. If a track was matched within p_T-dependent thresholds ranging from $(\Delta\eta, \Delta\varphi) \approx (0.037, 0.084)$ at $p_T = 0.15$ GeV/c to $(\Delta\eta, \Delta\varphi) \approx (0.010, 0.015)$ at $p_T = 100$ GeV/c, then a hadronic correction was applied to the cluster: $E_{\mathrm{cluster}}^{\mathrm{hadcorr}} = E_{\mathrm{cluster}}^{\mathrm{nonlincorr}} - \Delta E$, where $E_{\mathrm{cluster}}^{\mathrm{nonlincorr}}$ is the nonlinearity corrected cluster energy, and $\Delta E = c \sum_i p_i^{\mathrm{track}}$, where i spans all tracks matched to the cluster, p_i^{track} is the track three-momentum, and c is the speed of light. After the above cuts and corrections were performed, clusters with $E_{\mathrm{cluster}}^{\mathrm{hadcorr}} > 300$ MeV were accepted.

TABLE I. Approximate values characterizing the jet reconstruction performance for $R = 0.2$ and $R = 0.4$ in pp and Pb-Pb collisions. For cases with a leading track requirement, $p_{\mathrm{T}}^{\mathrm{lead,ch}} = 5$ GeV/c is used for $R = 0.2$ and $p_{\mathrm{T}}^{\mathrm{lead,ch}} = 7$ GeV/c for $R = 0.4$.

$p_{\mathrm{T,jet}}$	pp ($p_{\mathrm{T}}^{\mathrm{lead,ch}} > 0$ GeV/c)		pp ($p_{\mathrm{T}}^{\mathrm{lead,ch}} > 5/7$ GeV/c)		Pb-Pb ($p_{\mathrm{T}}^{\mathrm{lead,ch}} > 5/7$ GeV/c)	
	20 GeV/c	100 GeV/c	20 GeV/c	100 GeV/c	20 GeV/c	100 GeV/c
$R = 0.2$						
Δ_{JES}	-29%	-30%	-18%	-28%	-23%	-35%
JER	27%	21%	19%	19%	35%	23%
$\varepsilon_{\mathrm{reco}}$	98%	100%	86%	96%	86%	96%
$R = 0.4$						
Δ_{JES}	-30%	-31%	-14%	-27%	-6%	-33%
JER	23%	18%	15%	16%	77%	25%
$\varepsilon_{\mathrm{reco}}$	99%	100%	82%	92%	82%	92%

III. JET RECONSTRUCTION

Jets were reconstructed with $R = 0.1$–0.6 in pp collisions and $R = 0.2, 0.4$ in Pb-Pb collisions using the anti-k_{T} sequential recombination algorithm implemented in FAST-JET 3.2.1 [62,63] from the combination of charged particle tracks and hadronically corrected EMCal clusters. We used the p_{T} recombination scheme, assuming EMCal clusters are massless: $p_{\mathrm{T,jet}}^{\mathrm{raw}} = \sum_i p_{\mathrm{T,track}}^i + \sum_j p_{\mathrm{T,cluster}}^j$, where $p_{\mathrm{T,cluster}} = E_{\mathrm{cluster}}^{\mathrm{hadcorr}}/c$.

In Pb-Pb collisions, we subtracted the average combinatorial background following the approach in Ref. [9]. The background density ρ was determined in each event and used to subtract the average background from each jet in that event: $p_{\mathrm{T,jet}}^{\mathrm{reco}} = p_{\mathrm{T,jet}}^{\mathrm{raw}} - \rho A$, where A is the jet area. The average background density in 0–10% central events is typically $\langle \rho \rangle \approx 220$–$280$ GeV/c, corresponding to ≈ 110–140 GeV/c for a $R = 0.4$ jet. In pp collisions, we did not subtract the background due to the underlying event, in order to minimize the model dependence of the measurement.

Jets selected for the measurement were required to satisfy several criteria in order to be accepted: (i) the center of the jet must be within the fiducial volume of the EMCal, i.e., a distance $\Delta R \equiv \sqrt{(\Delta\eta)^2 + (\Delta\varphi)^2}$ from any edge of the EMCal, (ii) the jet must not contain any tracks with $p_{\mathrm{T,track}} > 100$ GeV/c, (iii) in Pb-Pb and applicable pp results, the jet must contain a track with $p_{\mathrm{T,track}} > 5$–7 GeV/c, depending on R, and (iv) in Pb-Pb collisions, the area of the jet must be $A > 0.6\pi R^2$. The $p_{\mathrm{T,track}} < 100$ GeV/c requirement removed only a small number of jets at large $p_{\mathrm{T,jet}}^{\mathrm{reco}}$ and has negligible bias for the $p_{\mathrm{T,jet}}^{\mathrm{reco,max}}$ selected in this analysis. The leading track requirement introduces a small fragmentation bias in the jet sample, which may lead to a bias in the measured jet suppression. This effect is discussed in Sec. VI and is estimated to have only a small effect on the reported R_{AA}. A larger leading track requirement is needed for larger R since the magnitude of background fluctuations increases with R. The area cut in Pb-Pb collisions was negligible except at very low $p_{\mathrm{T,jet}}^{\mathrm{reco}}$, where it rejects combinatorial jets.

In Pb-Pb collisions, local fluctuations in the background smear the reconstructed jet momentum. To study jet-by-jet fluctuations in the background, we generated a random

(η, φ) within the fiducial calorimeter acceptance in each event and compared the sum of constituents in a cone of radius R to the expected average background in that cone: $\delta_{p_{\mathrm{T}}} = \sum_{\mathrm{cone}} (p_{\mathrm{T,track}} + p_{\mathrm{T,cluster}}) - \rho\pi R^2$. The width of the $\delta_{p_{\mathrm{T}}}$ distribution is a measure of the size of the background fluctuations [64]. For $R = 0.2$, the standard deviation of the $\delta_{p_{\mathrm{T}}}$ distribution is $\sigma_{\delta_{p_{\mathrm{T}}}} = 6.5$ GeV/c, which grows to $\sigma_{\delta_{p_{\mathrm{T}}}} = 16.1$ GeV/c for $R = 0.4$. In the present analysis, the $\delta_{p_{\mathrm{T}}}$ distributions were not explicitly used except to determine the $p_{\mathrm{T,jet}}^{\mathrm{reco}}$ range to utilize in the analysis, which is discussed in Sec. IV.

We evaluated the performance of our jet reconstruction strategy by estimating the mean jet energy scale shift, $\Delta_{\mathrm{JES}} = \langle (p_{\mathrm{T,jet}}^{\mathrm{reco}} - p_{\mathrm{T,jet}}^{\mathrm{true}})/p_{\mathrm{T,jet}}^{\mathrm{true}} \rangle$, the jet energy resolution, $\mathrm{JER} = \sigma(p_{\mathrm{T,jet}}^{\mathrm{reco}})/p_{\mathrm{T,jet}}^{\mathrm{true}}$, and the jet reconstruction efficiency, $\varepsilon_{\mathrm{reco}}$, from PYTHIA8 MONASH 2013 and the ALICE detector simulation. Table I shows approximate values of Δ_{JES}, JER, and $\varepsilon_{\mathrm{reco}}$ for $R = 0.2$ and $R = 0.4$ in pp and Pb-Pb collisions. The jet energy scale shift is a long-tailed asymmetric distribution due to reconstruction inefficiency (such as tracking inefficiency) [10], and Δ_{JES} should be understood only as a rough characterization of this distribution. When a leading track requirement is imposed, the jet reconstruction efficiency and jet energy scale shift are primarily due to this requirement in combination with the tracking efficiency. Note that the pp response approximately, but not exactly, describes the detector effects in jet reconstruction relevant for Pb-Pb collisions. In Pb-Pb collisions, the jet reconstruction performance (including the effect of background fluctuations) was determined by embedding pp MC events into Pb-Pb data, as described in detail in Sec. IV. The JER is approximately constant at $\approx 23\%$ above $p_{\mathrm{T,jet}}^{\mathrm{true}} = 60$ GeV/c for $R = 0.2$, and deteriorates at lower $p_{\mathrm{T,jet}}^{\mathrm{true}}$ due to background fluctuations. As R increases, the JER deteriorates due to the increased influence of background fluctuations.

IV. CORRECTIONS

The reconstructed $p_{\mathrm{T,jet}}^{\mathrm{reco}}$ spectrum includes fluctuations in the underlying background (in Pb-Pb collisions) and a variety of detector effects, including tracking inefficiency, missing long-lived neutral particles (n, $\mathrm{K}_{\mathrm{L}}^0$), and particle-material

interactions. We therefore deconvoluted the reconstructed jet spectrum with a response matrix (RM) describing the correlation between $p_{\mathrm{T,jet}}^{\mathrm{reco}}$ and $p_{\mathrm{T,jet}}^{\mathrm{true}}$ in order to recover the "truth"-level jet spectrum at the hadron level.

In *pp* collisions, we generated a RM using PYTHIA8 MONASH 2013 with the full GEANT3 ALICE detector simulation, based on the detector performance in the relevant 2017 *pp* data-collection period. In Pb-Pb collisions, we generated a RM by embedding PYTHIA events (with detector simulation based on the detector performance in the 2015 Pb-Pb data-collection period) into Pb-Pb data after the detector-level reconstruction was run individually on both. The set of tracks in the "hybrid" event was taken as the sum of all tracks in both events individually, while the set of EMCal clusters were reclustered from a combined pool of cells from both events. This embedding-based approach, which uses real background, ensures that the detector response accurately reflects the Pb-Pb response of the calorimeter, including particle overlaps in the calorimeter as well as the Pb-Pb particle composition, and ensures the effect of the hadronic correction is equivalent in data and in the response. Moreover, it ensures that the correlation between the local background and the reconstructed jet due to local detector inefficiencies is accounted for.

The truth-level jet was constructed from the primary particles of the PYTHIA event, defined as all particles with a proper decay length longer than 1 cm, excluding daughters of these particles [65]. We correct the jet p_{T} to include the "missing" long-lived neutral particles.

The detector-level jet in *pp* collisions was constructed from the PYTHIA tracks and clusters at detector level. In Pb-Pb collisions, the detector-level jet was constructed from the "hybrid" event consisting of both PYTHIA and Pb-Pb tracks and clusters at detector level. To account for the decreased tracking efficiency in Pb-Pb collisions, we randomly rejected 2% of the PYTHIA tracks in the Pb-Pb case, independent of p_{T}. The average combinatorial background was subtracted as in 0–10% central Pb-Pb data: We computed the event-by-event ρ_{charged} using only Pb-Pb tracks, and we applied the background scale factor obtained in Pb-Pb data; we assume that the combinatorial background from the *pp* event is negligible.

In order to fill the RM, we matched truth-level jets to detector-level jets by a geometrical matching procedure. In *pp* collisions, if an accepted detector-level jet and an accepted PYTHIA jet were within $\Delta R < 0.6R$, and they were both the closest jets to each other, then the jets were matched, and they contribute to the RM. In Pb-Pb collisions, if an accepted hybrid jet and an accepted PYTHIA jet were within $\Delta R < 1.5R$, and they were both the closest jets to each other, then the jets were matched, and they contribute to the RM. The leading track requirement nullifies the need in Pb-Pb collisions for further criteria such as a shared momentum fraction requirement in order to generate accurate matches. The RM was generated with 5 GeV/c bin widths for $p_{\mathrm{T,jet}}^{\mathrm{reco}}$ and 10 GeV/c widths for $p_{\mathrm{T,jet}}^{\mathrm{true}}$ and was normalized so as to preserve the number of jets upon unfolding.

To perform the deconvolution, we employed the SVD unfolding algorithm [66] using the ROOUNFOLD package [67]. The regularization parameter k suppresses high-frequency variations in the unfolded result and was

TABLE II. Minimum and maximum reconstructed jet p_{T} used in the analysis as input to the deconvolution procedure.

	pp (GeV/c)		Pb-Pb (GeV/c)	
	$p_{\mathrm{T,jet}}^{\mathrm{reco,min}}$	$p_{\mathrm{T,jet}}^{\mathrm{reco,max}}$	$p_{\mathrm{T,jet}}^{\mathrm{reco,min}}$	$p_{\mathrm{T,jet}}^{\mathrm{reco,max}}$
$R = 0.2$	7	130	20	120
$R = 0.4$	10	130	35	120

selected by examining the so-called *d*-vector distribution. Statistical uncertainties were computed according to MC pseudoexperiments within ROOUNFOLD. The reconstructed spectrum was input to the unfolding procedure over a fixed window of $p_{\mathrm{T,jet}}^{\mathrm{reco}} \in [p_{\mathrm{T,jet}}^{\mathrm{reco,min}}, p_{\mathrm{T,jet}}^{\mathrm{reco,max}}]$, as illustrated in Table II. In Pb-Pb collisions, each of these $p_{\mathrm{T,jet}}^{\mathrm{reco,min}}$ corresponds to ≈ 2–$3 \times \sigma_{\delta_{p_T}}$, which, in combination with the leading charged hadron requirement, results in a sample largely free of combinatorial jets. A larger value of $p_{\mathrm{T,jet}}^{\mathrm{reco,min}}$ was used in Pb-Pb collisions in order to minimize the impact of the combinatorial background, which can destabilize the unfolding process. Any residual combinatorial jets will still be unfolded to low p_{T} by the RM. Since truncating the RM in $p_{\mathrm{T,jet}}^{\mathrm{reco}}$ loses the information of the fraction of truth-level jets that migrate outside of the measured detector-level window, we corrected for this kinematic efficiency. The unfolded result is then reported in a range over which the input data provides meaningful constraints, that is, a region unaffected by combinatorial jets and where the kinematic efficiency is larger than approximately 80%.

We corrected the unfolded spectrum for the fact that the jet finding procedure failed to reconstruct a certain fraction of jets. We computed the jet reconstruction efficiency as

$$\varepsilon_{\mathrm{reco}}\left(p_{\mathrm{T,jet}}^{\mathrm{true}}\right) = N_{\mathrm{matched}}\left(p_{\mathrm{T,jet}}^{\mathrm{true}}\right) / N_{\mathrm{truth}}\left(p_{\mathrm{T,jet}}^{\mathrm{true}}\right),$$

where N_{matched} is the number of accepted detector-level jets matched to PYTHIA truth-level jets out of N_{truth} accepted truth-level jets. In order that $\varepsilon_{\mathrm{reco}}$ also includes the false positive rate of accepted detector-level jets that have no matching truth-level jet (which can occur if the truth-level jet was generated slightly outside of our geometrical acceptance), the numerator also contains matches to truth-level jets outside of the EMCal fiducial acceptance. Note that $\varepsilon_{\mathrm{reco}}$ does not explicitly include the bias of the leading charged hadron requirement, but only the probability to reconstruct an accepted jet given a truth-level jet satisfying the leading charged hadron requirement (when applicable). In order for $\varepsilon_{\mathrm{reco}}$ to be the jet reconstruction efficiency, the jet matching efficiency must be 100%. However, in the Pb-Pb embedding environment, this is difficult to achieve, since some criteria need to be imposed to suppress combinatorial jets (in our case, the leading track requirement). Therefore, in the Pb-Pb case we used the jet reconstruction efficiency as determined from a *pp* simulation alone (with 2% reduced tracking efficiency).

The unfolded solution was verified to be mathematically robust by performing a refolding test and a "self-closure" test. The refolding test consisted of generating a RM (from half of the MC data sample runs) and unfolding the measured

distribution, then applying a RM (from the other half of the MC data sample) to the unfolded result, and comparing the refolded solution to the measured distribution. The self-closure test consisted of taking the matched detector-level jet spectrum in the full embedded sample and smearing each data point with a Gaussian according to the statistical uncertainties of the measured data. This spectrum was then unfolded using the RM and compared the result to the truth-level PYTHIA jet spectrum. In both cases, consistency was achieved within statistical uncertainties.

In Pb-Pb collisions, the unfolded solution is verified to be physically correct by a thermal model closure test similar to that in Ref. [9]. The closure test consisted of performing the entire analysis on "hybrid" events containing a PYTHIA event and a thermal background, in which "hybrid" jets were clustered from the combination of PYTHIA detector-level particles and thermal background particles. The background was modeled by generating N particles from a Gaussian, with p_T taken from a Γ distribution, $f_\Gamma(p_T; \beta) \sim p_T e^{-p_T/\beta}$, where the free parameters $\overline{N}, \sigma_N, \beta$ were fixed to roughly fit the δ_{p_T} distribution in 0–10% Pb-Pb data. The test consisted of constructing the hybrid detector-level jet spectrum, building the RM, unfolding the hybrid jets—and comparing the spectrum to the truth-level PYTHIA spectrum. Since the background does not have any jet component, this test is able to verify whether the analysis procedure indeed recovers the jet spectrum and is not contaminated by combinatorial jets. These tests validated the analysis procedure within approximately 5% for $R = 0.2$ with $p_T^{\text{lead,ch}} = 5$ GeV/c and $R = 0.4$ with $p_T^{\text{lead,ch}} = 7$ GeV/c.

V. SYSTEMATIC UNCERTAINTIES

Following Ref. [9], we categorized two classes of systematic uncertainties: correlated uncertainties and shape uncertainties. Correlated uncertainties encompass detector effects such as uncertainty on the tracking efficiency and uncertainty on the EMCal response, which are approximately fully positively correlated among all $p_{T,\text{jet}}$ bins. Shape uncertainties refer to systematic unfolding uncertainties, which alter the shape of the final $p_{T,\text{jet}}$ spectrum. The dominant systematic uncertainties in this analysis are the uncertainty in the tracking efficiency and the systematic uncertainty in the unfolding procedure. Note that in general the following uncertainties describe uncertainties on the jet yield, not on the jet p_T scale.

A. Correlated uncertainties

The dominant correlated uncertainty is the uncertainty on the modeling of the tracking efficiency, since correcting for unmeasured tracks has a major effect on the unfolding procedure. For the track selection described in Sec. II, the uncertainty on the tracking efficiency is approximately 4%, as estimated from variation in the track selection parameters and variation in the ITS-TPC matching requirements. In order to assign a systematic uncertainty to the final result, we constructed a RM using the same techniques as for the final result except with an additional 4% of PYTHIA tracks randomly rejected in jet finding (for Pb-Pb, this is in addition to the 2% rejection used for the main result). The jet reconstruction

efficiency was also computed with this extra 4% suppression applied. This modified RM was then used to unfold the same measured spectrum as used for the main result. This varied result was corrected for the jet reconstruction efficiency and compared to the main result, with the differences in each bin taken as the uncertainty. Additionally, the uncertainty due to the tracking p_T resolution was approximately 1%.

Systematic uncertainties due to the modeling of the EMCal response were included in several ways. In order to describe the uncertainty in the MC description of the EMCal hadronic response, the subtracted energy in the hadronic correction was varied from 100% to 70% of the matched track momentum. Moreover, a systematic uncertainty associated with the track-matching criteria was included by changing the p_T-dependent track-matching criteria to p_T-independent criteria $\Delta\eta < 0.015$, $\Delta\varphi < 0.03$. These two uncertainties were combined in quadrature to form the uncertainty on the EMCal hadronic correction procedure. In order to describe the uncertainty in the MC description of the EMCal electromagnetic response, in the pp case the photon conversion based nonlinearity correction was switched off. These variations were individually performed both in the RM and the data, and the systematic uncertainty was evaluated by comparing the modified unfolded result to the main result. In the Pb-Pb case, there is an additional uncertainty due to the fact that the MC does not exactly describe the cluster energy nonlinearity. To account for this, different cluster nonlinearity corrections are typically applied to data and MC; however, in the Pb-Pb embedding procedure, the clusters are mixtures of data and MC cells. The main result was computed by applying the data nonlinearity parametrization to the mixed data and MC cells in the embedding procedure. Therefore, we applied the MC nonlinearity parametrization as a systematic variation. In Pb-Pb collisions for $R = 0.4$, the uncertainties on the EMCal nonlinearity correction and track matching procedure are large, primarily due to unfolding effects, which we do not decouple in the evaluation of the correlated uncertainties.

We included also a systematic uncertainty associated with the choice of jet matching procedure. For pp, the geometrical matching distance was varied from $0.4R$ to $0.8R$ (except for $R = 0.1$ from $0.2R$ to $0.9R$), which resulted in an uncertainty of less than 1% (1.5%). For Pb-Pb, we varied from a pure geometrical matching to an MC-fraction based approach, in which a shared momentum fraction requirement ensures that the matched jet contains more than 50% of the p_T of the MC jet. This gave an uncertainty of 2–6%.

We included also a systematic uncertainty associated with the model-dependent reliance on PYTHIA to unfold the spectra. In pp collisions, we reweighted the response matrix according to the jet angularity ($g = \sum_i p_{T,i} r_i / p_{T,\text{jet}}$, where $r_i = \sqrt{\Delta\eta^2 + \Delta\varphi^2}$ is the distance of the ith constituent from the jet axis) at truth level. Specifically, we re-weighted the response matrix such that the 50% largest angularity jets were weighted an additional $\pm 30\%$ relative to the 50% lowest angularity jets. This contributed an uncertainty ranging from $\approx 2\%$ to 7% depending on the jet R, and roughly independent of p_T. The same uncertainties were taken for Pb-Pb collisions.

Tables III and IV illustrate the contributions of the various correlated uncertainties for pp and Pb-Pb collisions. These

TABLE III. Summary of correlated systematic uncertainties on the pp jet spectra without a leading track bias, for select R. The columns $p_{\mathrm{T,jet}}^{\min}$ and $p_{\mathrm{T,jet}}^{\max}$ are the uncertainties at the minimum and maximum $p_{\mathrm{T,jet}}$ bin.

| | Relative uncertainty (%) | | | | | |
| | $R = 0.2$ | | | $R = 0.6$ | | |
pp	$p_{\mathrm{T,jet}}^{\min}$	$p_{\mathrm{T,jet}}^{\max}$	Avg.	$p_{\mathrm{T,jet}}^{\min}$	$p_{\mathrm{T,jet}}^{\max}$	Avg.
Tracking efficiency	5.9	9.1	7.7	9.4	8.9	9.0
Track p_{T} resolution	1.0	1.0	1.0	1.0	1.0	1.0
EMCal nonlinearity	0.5	0.5	0.5	1.0	0.9	1.0
Hadronic correction	0.2	1.2	0.5	1.2	2.1	0.9
Jet matching	0.1	0.0	0.0	0.2	0.2	0.2
PYTHIA fragmentation	0.5	1.0	0.4	3.1	5.6	5.8
Total corr. uncertainty	6.0	9.3	7.8	10.1	10.8	10.8

uncertainties are expected to be largely independent, so we summed their uncertainties in quadrature.

B. Shape uncertainties

In order to assign a shape uncertainty arising from the unfolding regularization procedure, we performed several systematic variations:

(1) Variation of the unfolding algorithm: We unfolded with a Bayes-inspired iterative unfolding algorithm [68].

(2) Variation of the regularization parameter: In the SVD unfolding, we varied the regularization parameter k one unit above and below the nominal solution.

(3) Variation of the prior: The SVD algorithm requires a prior distribution as input, which for the main result is the projection of the RM onto the truth axis (before normalization). We varied this input prior either by scaling the main prior by $p_{\mathrm{T}}^{\pm 0.5}$ or replacing it with a jet cross section produced by POWHEG or the unfolded main result itself.

(4) Variation of the input range: For Pb-Pb (pp) collisions, we varied the measured input range ± 5 ($^{+5}_{-3}$) GeV/c around the nominal value for each R.

The total shape uncertainty is then the standard deviation of the variations, $\sqrt{\sum_{i=1}^{3} \sigma_i^2 / 4}$, where σ_i is the systematic due to

a single variation, since they each comprise independent measurements of the same underlying systematic uncertainty in the regularization. Tables V and VI illustrate the contributions of the various shape uncertainties for pp and Pb-Pb collisions.

C. Uncertainties on the jet cross-section ratio

We computed the correlated systematic uncertainties on the pp jet cross-section ratio by making the same variations as in Sec. V A on both spectra simultaneously and compared the varied jet cross-section ratio to the main result. This resulted in significant cancellation of the correlated uncertainties between the numerator and denominator, as can be seen in Sec. VI. We computed the shape systematic uncertainties by adding the single spectra shape uncertainties in quadrature.

It is important to note that the statistical uncertainties of the numerator and denominator are partially correlated, due to error propagation through the unfolding procedure. We did not, however, take this into account. This may result in a slightly conservative statistical uncertainty estimation, since there may be significant cancellation between the two radii. Additionally, we did not use statistically independent samples to form the ratio, and so the numerator and denominator are statistically correlated with each other, which may lead to further slight overestimation of the statistical uncertainties.

TABLE IV. Summary of correlated systematic uncertainties on the Pb-Pb jet spectra, for select R and $p_{\mathrm{T}}^{\mathrm{lead,ch}}$ thresholds. The columns $p_{\mathrm{T,jet}}^{\min}$ and $p_{\mathrm{T,jet}}^{\max}$ are the uncertainties at the minimum and maximum $p_{\mathrm{T,jet}}$ bin.

| | Relative uncertainty (%) | | | | | |
| | $R = 0.2$, 5 GeV/c | | | $R = 0.4$, 7 GeV/c | | |
Pb-Pb	$p_{\mathrm{T,jet}}^{\min}$	$p_{\mathrm{T,jet}}^{\max}$	Avg.	$p_{\mathrm{T,jet}}^{\min}$	$p_{\mathrm{T,jet}}^{\max}$	Avg.
Tracking efficiency	5.8	8.9	8.0	9.9	9.8	9.8
Track p_{T} resolution	1.0	1.0	1.0	1.0	1.0	1.0
EMCal nonlinearity	2.1	1.1	1.6	11.4	7.9	9.5
Hadronic correction	0.8	5.9	2.0	12.8	9.9	12.4
Jet matching	2.0	2.0	2.0	6.0	2.0	2.8
PYTHIA fragmentation	0.8	3.6	2.0	2.8	5.1	3.8
Total corr. uncertainty	6.7	11.6	9.2	20.9	16.9	19.5

TABLE V. Summary of shape systematic uncertainties on the *pp* jet spectra without a leading track bias, for select R. The columns $p_{\mathrm{T,jet}}^{\min}$ and $p_{\mathrm{T,jet}}^{\max}$ are the uncertainties at the minimum and maximum $p_{\mathrm{T,jet}}$ bin.

| | Relative uncertainty (%) | | | | | |
| | $R = 0.2, 0 \,\mathrm{GeV}/c$ | | | $R = 0.6, 0 \,\mathrm{GeV}/c$ | | |
pp	$p_{\mathrm{T,jet}}^{\min}$	$p_{\mathrm{T,jet}}^{\max}$	Avg.	$p_{\mathrm{T,jet}}^{\min}$	$p_{\mathrm{T,jet}}^{\max}$	Avg.
Unfolding method	0.0	16.0	3.4	2.6	16.0	4.5
Reg. parameter	0.7	2.4	1.3	1.0	3.5	2.1
Prior	1.3	0.8	0.9	0.9	3.7	2.0
Input p_{T} range	0.8	3.3	1.3	0.4	3.2	1.4
Total shape uncertainty	0.8	8.3	2.2	1.5	8.5	3.0

VI. RESULTS

A. Inclusive jet spectra

1. pp

We report the *pp* full jet cross section for $R = 0.1, 0.2, 0.3, 0.4, 0.5, 0.6$ in Fig. 1 (left). The cross sections are reported differentially in $p_{\mathrm{T,jet}}$ and η_{jet} as $\frac{d^2\sigma_{\mathrm{jet}}}{dp_{\mathrm{T,jet}}d\eta_{\mathrm{jet}}} = \frac{1}{\mathcal{L}}\frac{d^2N}{dp_{\mathrm{T,jet}}d\eta_{\mathrm{jet}}}$, where we experimentally measured the yield $\frac{d^2N}{dp_{\mathrm{T,jet}}d\eta_{\mathrm{jet}}}$ and the integrated luminosity $\mathcal{L}$ [55]. The uncertainty on the luminosity is 2.1%. The measured jet cross sections were unfolded for detector and background effects and are reported at the hadron-level. The cross sections were corrected for the kinematic efficiency and jet reconstruction efficiency, as well as the partial azimuthal acceptance of the EMCal and the vertex efficiency. Note that a leading track requirement was not imposed for the results in Fig. 1.

We compare the *pp* inclusive jet cross section to two theoretical calculations in Fig. 1 (right). The predictions denoted NLO+NLL+NP are analytical predictions at NLO with resummation of jet R logarithms and threshold logarithms to NLL accuracy, performed in a rigorous QCD factorization scheme [28,30,31]. The effect of unaccounted higher order corrections was evaluated by various scale variations and is included as a systematic uncertainty. A correction for hadronization and multiparton interaction (MPI) effects is applied to this prediction, based on PYTHIA8 tune A14 and is shown in Fig. 2. These nonperturbative (NP) effects become large for low $p_{\mathrm{T,jet}}$ at both small and large R, where systematic uncertainties in this correction (beyond the scope

of this article) are likely critical. The predictions use PDF set CT14nlo. These predictions are seen to be generally consistent with the data, except at low p_{T} and small R. This tension may be due to the model-dependent NP correction, which is large in this region. The experimental data presented in Fig. 1, which cover a large range of R down to low p_{T} and therefore span a wide range of NP effects (from hadronization dominated at small R to MPI dominated at large R, as seen in Fig. 2), can be used to further constrain NP effects in *pp* collisions. This is of relevance both for *pp* QCD physics and for interpreting modifications in heavy-ion collisions, which are typically strongest at low p_{T}.

The predictions denoted POWHEG+PYTHIA8 consist of a MC parton-shower-based model using NLO calculations from POWHEG [69] matched to a parton shower and hadronization from PYTHIA8 tune A14.[1] Two theoretical uncertainties were computed for these predictions, both in regard to the POWHEG event generation: PDF uncertainty, computed as in Ref. [73], and scale uncertainty, which was computed by varying the

---

[1]The POWHEG reference was produced by POWHEG-BOX-V2 at $\sqrt{s} = 5.02\,\mathrm{TeV}$ via the jet pair production process [69–71]. PDF set CT14nlo was used, along with the settings bornktmin = 1 and bornsuppfact = 70. PYTHIA 8.2 tune A14 NNPDF2.3LO was used for the parton shower, which is tuned with ATLAS *pp* collisions at $\sqrt{s_{NN}} = 7\,\mathrm{TeV}$ using underlying event observables, jet substructure observables, and several other observables, not including the inclusive jet cross section [72]. Merging with PYTHIA was done as in Ref. [73]. The same set of primary particles was used as described earlier [65].

TABLE VI. Summary of shape systematic uncertainties on the Pb-Pb jet spectra, for select R and $p_{\mathrm{T}}^{\mathrm{lead,ch}}$ thresholds. The columns $p_{\mathrm{T,jet}}^{\min}$ and $p_{\mathrm{T,jet}}^{\max}$ are the uncertainties at the minimum and maximum $p_{\mathrm{T,jet}}$ bin.

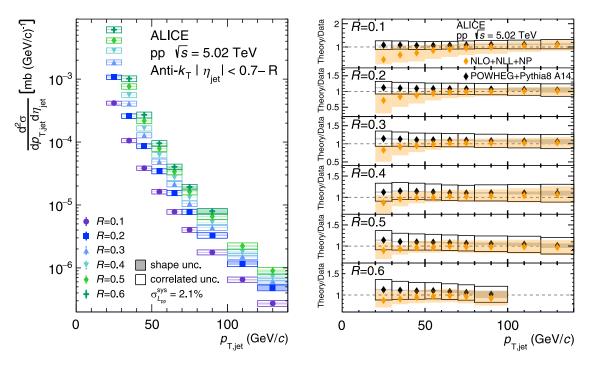| | Relative uncertainty (%) | | | | | |
| | $R = 0.2, 5 \,\mathrm{GeV}/c$ | | | $R = 0.4, 7 \,\mathrm{GeV}/c$ | | |
Pb-Pb	$p_{\mathrm{T,jet}}^{\min}$	$p_{\mathrm{T,jet}}^{\max}$	Avg.	$p_{\mathrm{T,jet}}^{\min}$	$p_{\mathrm{T,jet}}^{\max}$	Avg.
Unfolding method	7.7	10.0	5.4	30.3	2.5	18.2
Reg. parameter	4.2	8.7	4.4	24.9	20.6	23.1
Prior	1.5	6.7	2.4	2.3	8.3	4.2
Input p_{T} range	0.4	0.9	0.6	1.5	1.7	1.4
Total shape uncertainty	4.4	7.4	3.8	19.6	11.2	15.5

FIG. 1. Left: Unfolded *pp* full jet cross section at $\sqrt{s} = 5.02$ TeV for $R = 0.1$–0.6. No leading track requirement is imposed. Right: Ratio of NLO+NLL+NP and POWHEG+PYTHIA8 tune A14 predictions to the measured data. The systematic uncertainties in the ratio are denoted by boxes and are the quadratic sum of the systematic uncertainties in data and the predictions. Note that no systematic uncertainties for the nonperturbative correction in the NLO+NLL+NP prediction were included.

renormalization and factorization scales. The total theoretical uncertainty on the cross section was obtained by adding these two contributions in quadrature. Note that large nonperturbative effects, similar to Fig. 2, are implicitly present in this

FIG. 2. Nonperturbative correction factor applied to parton-level NLO+NLL predictions, obtained from PYTHIA8 tune A14 as the ratio of the inclusive jet spectrum at hadron-level with MPI compared to parton-level without MPI.

prediction as well. The POWHEG+PYTHIA8 predictions are consistent with the measured data for all R and $p_{T,jet}$. Figure 1 does not include predictions by PYTHIA alone, since it is well established that NLO contributions are necessary to obtain the *pp* inclusive jet cross section [32,39].

Figure 3 shows the *pp* jet cross section ratio for various R, built from the spectra in Fig. 1. The top two panels show the ratios of $R = 0.2$ to other radii, and the bottom two panels show the ratios of $R = 0.1$ to other radii. The left panels also include comparisons to POWHEG+PYTHIA8, and the right panels include comparisons to NLO+NLL+NP. Correlated uncertainties largely cancel [40,74], which allows this observable to elucidate higher precision effects compared to the inclusive jet cross section. The systematic uncertainties on the POWHEG+PYTHIA8 prediction largely cancel as well, and the resulting high-precision comparisons show that the cross-section ratios are generally well-described by POWHEG+PYTHIA8. The systematic uncertainties in the NLO+NLL+NP prediction, however, do not substantially cancel, because the scale variations include variation of softer scales which are sensitive to nonperturbative effects; the NLO+NLL+NP predictions are consistent with the measured data within the size of these large theoretical uncertainties.

2. Pb-Pb

We report the 0–10% central Pb-Pb jet spectra for $R = 0.2$ and $R = 0.4$ in Fig. 4. The spectra are reported differentially in $p_{T,jet}$ and η_{jet} as $\frac{1}{\langle T_{AA} \rangle} \frac{1}{N_{event}} \frac{d^2 N_{jet}^{AA}}{dp_{T,jet} d\eta_{jet}}$, where $\langle T_{AA} \rangle \equiv \frac{\langle N_{coll} \rangle}{\sigma_{inel}^{NN}}$ is the ratio of the number of binary nucleon-nucleon collisions to the inelastic nucleon-nucleon cross section, computed in a Glauber model to be $\langle T_{AA} \rangle = 23.07 \pm 0.44$ (sys) mb^{-1} for

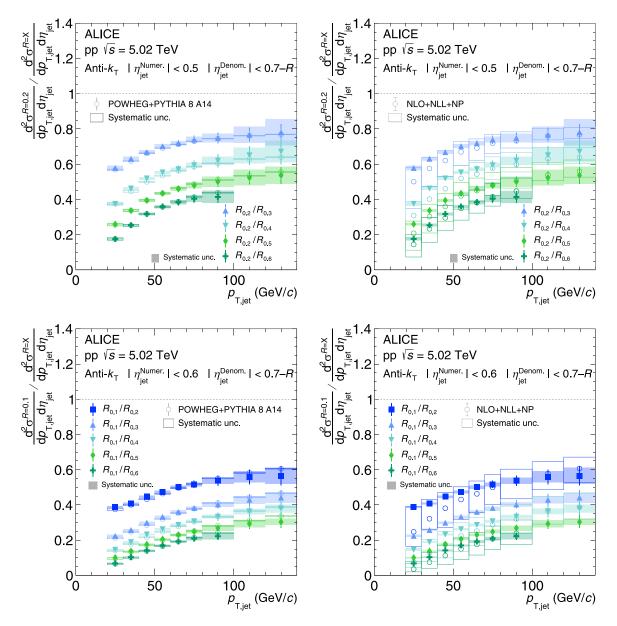FIG. 3. Unfolded pp jet cross-section ratios for various R. Top panels: ratios of $R = 0.2$ to other radii. Bottom panels: ratios of $R = 0.1$ to other radii. The left panels include comparisons to POWHEG+PYTHIA8, and the right panels include comparisons to NLO+NLL+NP. The experimental correlated systematic uncertainties and shape systematic uncertainties were combined in quadrature into a single systematic uncertainty. Note that no systematic uncertainties for the nonperturbative correction in the NLO+NLL+NP prediction were included.

0–10% centrality. The jet spectra were unfolded for detector and background effects, and are reported at the hadron level. The spectra were corrected for the kinematic efficiency and jet reconstruction efficiency, as well as the partial azimuthal acceptance of the EMCal. The $R = 0.2$ jets are reported for the range $p_{T,jet} \in [40, 140]$ GeV/c. The $R = 0.4$ jets are reported for the range $p_{T,jet} \in [60, 140]$ GeV/c. The reported intervals were selected based on being insensitive to the combinatorial background, as well as having kinematic efficiency above approximately 80%. Note that the reported $p_{T,jet}$ intervals extend higher than the measured $p_{T,jet}^{reco}$ range because the kinematic efficiency remains high at larger $p_{T,jet}$ due to the JES shift. A leading track bias of 5 GeV/c was required for the $R = 0.2$ spectra, while a 7 GeV/c bias was required for

the $R = 0.4$ spectra (both pp reference and Pb-Pb) in order to suppress combinatorial jets in Pb-Pb collisions. We did not attempt to correct to a fully inclusive spectrum, in order to avoid model dependence. The pp cross sections with leading track biases of 5 and 7 GeV/c are plotted alongside the Pb-Pb spectra in Fig. 4.

B. Jet R_{AA}

We report the jet R_{AA} as

$$R_{AA} = \frac{\frac{1}{N_{event}} \frac{d^2N}{dp_{T,jet} d\eta_{jet}}\Big|_{AA}}{\langle T_{AA} \rangle \frac{d^2\sigma}{dp_{T,jet} d\eta_{jet}}\Big|_{pp}},$$
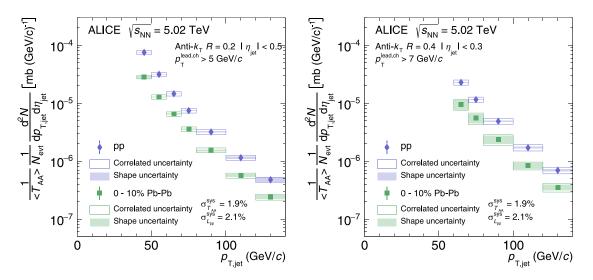
FIG. 4. Unfolded *pp* and Pb-Pb full jet spectra at $\sqrt{s_{NN}} = 5.02$ TeV for $R = 0.2$ (left), with 5 GeV/*c* leading track requirement, and $R = 0.4$ (right), with 7 GeV/*c* leading track requirement. The *pp* data points correspond to $\frac{d^2\sigma}{dp_{T,\text{jet}} d\eta_{\text{jet}}}$.

namely the ratio of the Pb-Pb and *pp* spectra plotted above. While the measured Pb-Pb spectra only report jets satisfying the leading charged hadron requirement, one can choose whether or not to apply the same requirement for the *pp* reference, even though the bias may be different in *pp* and Pb-Pb collisions. To examine the effect of this bias, in Fig. 5 we plot the ratio of the $R = 0.2$ *pp* cross section with either a 0, 5, or 7 GeV/*c* leading track requirement, as well as the ratio of the $R = 0.2$ Pb-Pb jet spectrum with either a 5- or 7-GeV/*c* leading track requirement. Figure 5 shows that the relative bias between 5- and 7-GeV/*c* leading track requirements is very similar in *pp* and Pb-Pb collisions, suggesting that the overall bias in the reported R_{AA} may be small compared to the measurement uncertainties. Nevertheless, we report the R_{AA} both with and without a leading track requirement on the *pp* reference.

Figure 6 shows the unfolded full jet R_{AA} for $R = 0.2$ and $R = 0.4$ jets, both with and without a leading track requirement on the *pp* reference. The uncertainties in the Pb-Pb and *pp* spectra were combined in quadrature. The jet R_{AA} exhibits strong suppression and constitutes the first 0–10% jet R_{AA} measurements at $\sqrt{s_{NN}} = 5.02$ TeV at low jet p_T (i.e., $p_{T,\text{jet}} < 100$ GeV/*c*), and the first inclusive jet R_{AA} measurements by ALICE extending to $R = 0.4$ at any collision energy. There is visible $p_{T,\text{jet}}$ dependence in the $R = 0.2$ case, with stronger suppression at lower $p_{T,\text{jet}}$. There is no significant R dependence of the jet R_{AA} within the experimental uncertainties. We do not report the jet cross-section ratio for different R in Pb-Pb collisions due to the fact that we found minimal cancellation of uncertainties (due to large unfolding uncertainties for
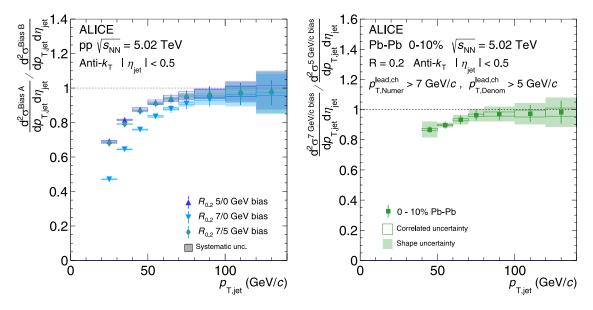

FIG. 5. Left: Ratio of the *pp* jet cross section with various leading charged particle requirements. Right: Ratio of the $R = 0.2$ Pb-Pb jet cross section with a 7 GeV/*c* leading charged particle requirement compared to a 5 GeV/*c* leading charged particle requirement.
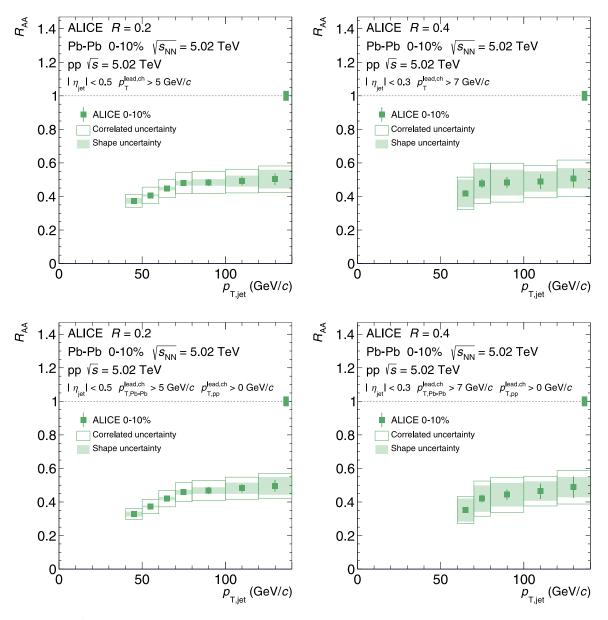
FIG. 6. Jet R_{AA} at $\sqrt{s_{NN}} = 5.02$ TeV for $R = 0.2$ (left) and $R = 0.4$ (right). In the top panel, a leading track requirement is imposed on the *pp* reference, while in the bottom panel no such requirement is imposed on the *pp* reference. The combined $\langle T_{AA} \rangle$ uncertainty and *pp* luminosity uncertainty of 2.8% is illustrated as a band on the dashed line at $R_{AA} = 1$.

$R = 0.4$), and it therefore does not convey additional information beyond the reported R_{AA}.

We compare these results to four theoretical predictions: the linear Boltzmann transport (LBT) model [25,75], soft collinear effective theory with Glauber gluons (SCET$_G$) [29,76–78], the hybrid model [79–82], and JEWEL [83,84]. The R_{AA} predictions of these models are compared to the measured data (with the leading track requirements imposed) in Fig. 7 for $R = 0.2$ and $R = 0.4$. The predictions were all computed using the anti-k_T jet algorithm with $|\eta_{jet}| < 0.7 - R$. Leading track requirements were only applied by JEWEL (as in data) and the hybrid model (with 5 GeV/c for both radii), for both *pp* and Pb-Pb collisions.

JEWEL is a Monte Carlo implementation of BDMPS jet energy loss with a parton shower, and allows the option

to include the recoiling thermal medium particles in the jet energy ("recoil on") or to ignore the recoiling medium particles ("recoil off") [24]. In the case of including the recoils, the recoil particles free stream and do not interact again with the medium. If recoils are included, we perform background subtraction according to the recommended option "4MomSub." JEWEL contains several free parameters that are fixed by independent measurements, none of which use high-p_T LHC measurements; we take $T = 440$ MeV and $t_0 = 0.4$ fm/c [84]. Note that these predictions do not include systematic uncertainties, but rather only statistical uncertainties.

The linear Boltzmann transport (LBT) model implements pQCD energy loss based on a higher twist gluon radiation spectrum induced by elastic scattering and describes the
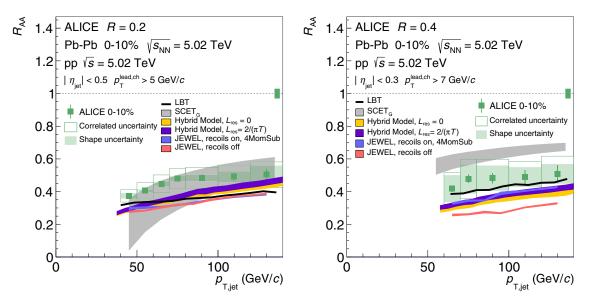
FIG. 7. Jet R_{AA} at $\sqrt{s_{NN}} = 5.02$ TeV for $R = 0.2$ (left) and $R = 0.4$ (right) compared to LBT, SCET$_G$, hybrid model, and JEWEL predictions. The combined $\langle T_{\mathrm{AA}} \rangle$ uncertainty and pp luminosity uncertainty of 2.8% is illustrated as a band on the dashed line at $R_{\mathrm{AA}} = 1$. Systematic uncertainties are only included for the SCET$_G$ and hybrid model predictions; see text for details.

evolution of jet and recoiling medium particles through the thermal medium with linear Boltzmann equations. An effective strong coupling constant α_s is taken as a free parameter fit to experimental data. The model calculations are performed according to the methods in Ref. [25]. No systematic uncertainties were provided for this calculation.

Soft collinear effective theory with Glauber gluons (SCET$_G$) builds on the approach of soft collinear effective theory (SCET), in which the jet cross section is factorized into a "hard function" corresponding to the initial scattering and a "jet function" corresponding to the fragmentation of a hard-scattered parton into a jet. In SCET$_G$, jet energy loss in heavy-ion collisions is implemented by interactions of jet partons with the hot QCD medium in an effective field theory via the exchange of "Glauber" gluons, encapsulated in an in-medium jet function. The predictions were performed according to Ref. [29] but with minor differences. The pp jet cross section was computed to NLO in α_s, and with a LL resummation in jet R. Medium effects were computed at NLO, but without a resummation in jet R (resulting in large systematic uncertainties for $R = 0.2$). The in-medium splitting functions described above include radiative processes evaluated using $2 + 1$D viscous hydrodynamics, but these predictions do not include collisional energy loss. Note that this could have significant impact particularly on the larger radius jets, where it may increase suppression. The EFT coupling constant between the medium and jets is $g = 2.0$. For pp collisions, the CT14nlo PDF was used, and for Pb-Pb collisions, the nCTEQ15FullNuc PDF was used. Energy loss in cold nuclear matter was also taken into account. The plotted error band represents the systematic uncertainty obtained by scale variations.

In the hybrid model, partons are produced by vacuum pQCD, and shower according to vacuum pQCD—but in between these hard splittings, parton energy loss is modeled according to a gauge-gravity duality computation in $N = 4$

supersymmetric Yang-Mills at infinitely strong coupling and large N_c. Model predictions were provided with two values of L_{res}, which describes the scale at which the medium can resolve two split partons. The medium evolution was modeled by a hydrodynamic expansion. The plotted error bands represent the combination of statistical and systematic uncertainties.

All models exhibit strong suppression and produce the same qualitative trend of R_{AA} as a function of $p_{\mathrm{T,jet}}$. In the case $R = 0.2$, JEWEL slightly underpredicts the jet R_{AA} regardless of whether medium recoils are included, while for $R = 0.4$ the "recoils on" prediction is more consistent with the data. There is no significant difference between the "recoil on" or "recoil off" option in JEWEL for $R = 0.2$; one expects in general a smaller impact from medium recoil in smaller radius jets. The LBT model describes the data marginally better, but still shows slight tension. Note that the dominant systematic uncertainties in the data are positively correlated between $p_{\mathrm{T,jet}}$ bins. Neither the JEWEL nor LBT predictions include systematic uncertainties. The SCET$_G$ predictions are consistent with the data, although the $R = 0.2$ prediction has large systematic uncertainties due to a lack of in-medium $\ln R$ resummation in this calculation. Additionally, the SCET$_G$ calculation did not include collisional energy loss, which may underestimate suppression for $R = 0.4$. The hybrid model describes the trend of the data reasonably well, although like the LBT model, it exhibits slight tension, particularly in the $p_{\mathrm{T,jet}} < 100$ GeV/c range. The shapes of the $p_{\mathrm{T,jet}}$ dependence differ between the model predictions, most notably between SCET$_G$ and the others. While the experimental uncertainties are larger for $R = 0.4$, the model predictions span a wider range of R_{AA} than in the case of $R = 0.2$, which highlights the importance of measuring the R dependence of the jet R_{AA}.

The predictions typically use different strategies for each of the "non jet energy loss" pieces (initial state, expansion, hadronization, pp reference spectrum) and do not attempt
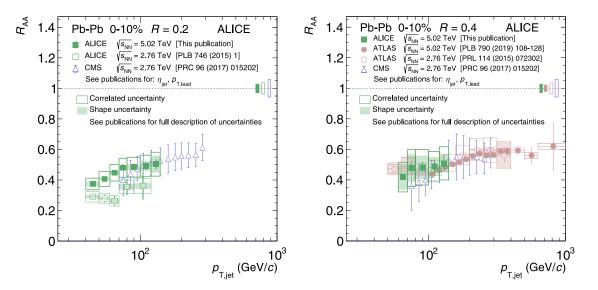
FIG. 8. Jet R_{AA} in 0–10% central Pb-Pb collisions for $R = 0.2$ (left) and $R = 0.4$ (right) for all currently published experimental results. Closed markers denote $\sqrt{s_{NN}} = 5.02$ TeV, and open markers denote $\sqrt{s_{NN}} = 2.76$ TeV.

to incorporate these differences in a systematic uncertainty, which makes a strict quantitative comparison to data difficult. Moreover, the models fix their free parameters in different ways; JEWEL has not been fit to high-$p_{T,jet}$ LHC data, and so it faces the strictest test of all the models presented. This necessitates investigation of complementary jet observables and global analyses, but it also highlights the need to standardize the ingredients of jet energy loss calculations [85]. The data presented here provide important constraints at low-$p_{T,jet}$ on current models as well as for future global analyses.

Figure 8 shows a comparison of the results in Fig. 6 (top) to all currently published experimental results of 0–10% central jet R_{AA} for $R = 0.2$ and $R = 0.4$. This comparison broadly illustrates that there is no clear R dependence or $\sqrt{s}$ dependence of the jet R_{AA} within current experimental precision. We do not attempt to comment on the comparison of theoretical models with global experimental results, which is beyond the scope of this article.

VII. CONCLUSION

We measured the transverse momentum (p_T) spectrum of jets in *pp* collisions at $\sqrt{s} = 5.02$ TeV and Pb-Pb collisions at $\sqrt{s_{NN}} = 5.02$ TeV, as well as the jet nuclear modification factor (R_{AA}), using charged particles from the tracking system combined with particle information from the electromagnetic calorimeter. We measured the inclusive jet cross section in *pp* collisions for jet resolution parameters $R = 0.1$–0.6, which is the largest collection of full jet R measured by ALICE to date. We compared these measurements to theoretical predictions at next to leading order (NLO) including either a resummation of large logarithms or a matched parton shower. Both predictions describe the data well except with slight tension at low-$p_{T,jet}$ for the resummation-based prediction, which may be due to either the perturbative calculation or the large non perturbative corrections at low $p_{T,jet}$. We also presented the ratios of jet cross sections of various R, which leverage partial cancellation

of systematic uncertainties to obtain high-precision constraints on the R dependence of the cross section; the two models considered generally describe these ratios well. These data, spanning a large range of R down to low p_T, contain sensitivities to different nonperturbative effects (from hadronization dominated at small R to underlying event dominated at large R) and can be used to constrain the contributions of pQCD, hadronization, and underlying event effects on the inclusive jet cross section. These data can further be used to constrain parton distribution functions and the strong coupling constant.

We measured the jet spectrum in Pb-Pb collisions for $R = 0.2$ and $R = 0.4$, which constitutes the first 0–10% jet R_{AA} measurements at $\sqrt{s_{NN}} = 5.02$ TeV at $p_{T,jet} < 100$ GeV/c, and the first inclusive jet R_{AA} measurements by ALICE extending to $R = 0.4$ at any collision energy. The measured jet spectrum in Pb-Pb collisions exhibits strong suppression compared to *pp* collisions, and for $R = 0.2$ the data show stronger suppression at lower $p_{T,jet}$ than at higher $p_{T,jet}$. There is no significant R dependence of the jet R_{AA} within the uncertainties of the measurement. Models are able to generally describe the trends of the data, but several models exhibit hints of disagreement with the measurements. These data provide additional constraints on jet quenching models in heavy-ion collisions, which can be used to extract medium properties such as the transverse momentum diffusion parameter, $\hat{q}$, as a function of the medium temperature and the jet p_T.

[1] B. V. Jacak and B. Muller, The exploration of hot nuclear matter, Science **337**, 310 (2012).

[2] B. Müller, J. Schukraft, and B. Wysłouch, First results from Pb+Pb collisions at the LHC, Annu. Rev. Nucl. Part. Sci. **62**, 361 (2012).

[3] P. Braun-Munzinger, V. Koch, T. Schäfer, and J. Stachel, Properties of hot and dense matter from relativistic heavy ion collisions, Phys. Rep. **621**, 76 (2016).

[4] W. Busza, K. Rajagopal, and W. van der Schee, Heavy ion collisions: The big picture, and the big questions, Ann. Rev. Nucl. Part. Sci. **68**, 339 (2018).

[5] K. Adcox *et al.* (PHENIX Collaboration), Formation of dense partonic matter in relativistic nucleus-nucleus collisions at RHIC: Experimental evaluation by the PHENIX Collaboration, Nucl. Phys. A **757**, 184 (2005).

[6] J. Adams *et al.* (STAR Collaboration), Experimental and theoretical challenges in the search for the quark-gluon plasma: The STAR Collaboration's critical assessment of the evidence from RHIC collisions, Nucl. Phys. A **757**, 102 (2005).

[7] B. Back *et al.* (PHOBOS Collaboration), The PHOBOS perspective on discoveries at RHIC, Nucl. Phys. A **757**, 28 (2005).

[8] I. Arsene *et al.* (BRAHMS Collaboration), Quark-gluon plasma and color glass condensate at RHIC? The perspective from the BRAHMS experiment, Nucl. Phys. A **757**, 1 (2005).

[9] J. Adam *et al.* (ALICE Collaboration), Measurement of jet suppression in central Pb-Pb collisions at $\sqrt{s_{NN}} = 2.76$ TeV, Phys. Lett. B **746**, 1 (2015).

[10] B. Abelev *et al.* (ALICE Collaboration), Measurement of charged jet suppression in Pb-Pb collisions at $\sqrt{s_{NN}} = 2.76$ TeV, J. High Energy Phys. 03 (2014) 013.

[11] J. Adam *et al.* (ALICE Collaboration), Measurement of jet quenching with semi-inclusive hadron-jet distributions in central Pb-Pb collisions at $\sqrt{s_{NN}} = 2.76$ TeV, J. High Energy Phys. 09 (2015) 170.

[12] L. Adamczyk *et al.* (STAR Collaboration), Measurements of jet quenching with semi-inclusive hadron+jet distributions in Au + Au collisions at $\sqrt{s_{NN}} = 200$ GeV, Phys. Rev. C **96**, 024905 (2017).

[13] G. Aad *et al.* (ATLAS Collaboration), Measurement of the jet radius and transverse momentum dependence of inclusive jet suppression in lead-lead collisions at $\sqrt{s_{NN}} = 2.76$ TeV with the ATLAS detector, Phys. Lett. B **719**, 220 (2013).

[14] M. Aaboud *et al.* (ATLAS Collaboration), Measurement of the nuclear modification factor for inclusive jets in Pb+Pb collisions at $\sqrt{s_{NN}} = 5.02$ TeV with the ATLAS detector, Phys. Lett. B **790**, 108 (2019).

[15] V. Khachatryan *et al.* (CMS Collaboration), Measurement of inclusive jet cross sections in *pp* and Pb-Pb collisions at $\sqrt{s_{NN}} = 2.76$ TeV, Phys. Rev. C **96**, 015202 (2017).

[16] S. Acharya *et al.* (ALICE Collaboration), Medium modification of the shape of small-radius jets in central Pb-Pb collisions at $\sqrt{s_{NN}} = 2.76$ TeV, J. High Energy Phys. 10 (2018) 139.

[17] S. Chatrchyan *et al.* (CMS Collaboration), Observation and studies of jet quenching in Pb-Pb collisions at $\sqrt{s_{NN}} = 2.76$ TeV, Phys. Rev. C **84**, 024906 (2011).

[18] M. Aaboud *et al.* (ATLAS Collaboration), Measurement of jet fragmentation in Pb-Pb and *pp* collisions at $\sqrt{s_{NN}} = 5.02$ TeV with the ATLAS detector, Phys. Rev. C **98**, 024908 (2018).

[19] K. M. Burke *et al.* (JET Collaboration), Extracting the jet transport coefficient from jet quenching in high-energy heavy-ion collisions, Phys. Rev. C **90**, 014909 (2014).

[20] G.-Y. Qin and X.-N. Wang, Jet quenching in high-energy heavy-ion collisions, Int. J. Mod. Phys. E **24**, 1530014 (2015).

[21] J.-P. Blaizot and Y. Mehtar-Tani, Jet structure in heavy ion collisions, Int. J. Mod. Phys. E **24**, 1530012 (2015).

[22] A. Majumder and M. van Leeuwen, The theory and phenomenology of perturbative QCD based jet quenching, Prog. Part. Nucl. Phys. **66**, 41 (2011).

[23] J.-W. Qiu, F. Ringer, N. Sato, and P. Zurita, Factorization of Jet Cross Sections in Heavy-Ion Collisions, Phys. Rev. Lett. **122**, 252301 (2019).

[24] R. Elayavalli and K. Zapp, Medium response in JEWEL and its impact on jet shape observables in heavy ion collisions, J. High Energy Phys. 07 (2017) 141.

[25] Y. He, S. Cao, W. Chen, T. Luo, L.-G. Pang, and X.-N. Wang, Interplaying mechanisms behind single inclusive jet suppression in heavy-ion collisions, Phys. Rev. C **99**, 054911 (2019).

[26] M. Dasgupta, F. Dreyer, G. P. Salam, and G. Soyez, Small-radius jets to all orders in QCD, J. High Energy Phys. 04 (2015) 039.

[27] M. Dasgupta, F. A. Dreyer, G. P. Salam, and G. Soyez, Inclusive jet spectrum for small-radius jets, J. High Energy Phys. 06 (2016) 057.

[28] Z.-B. Kang, F. Ringer, and I. Vitev, The semi-inclusive jet function in SCET and small radius resummation for inclusive jet production, J. High Energy Phys. 10 (2016) 125.

[29] Z.-B. Kang, F. Ringer, and I. Vitev, Inclusive production of small radius jets in heavy-ion collisions, Phys. Lett. B **769**, 242 (2017).

[30] X. Liu, S.-O. Moch, and F. Ringer, Threshold and Jet Radius Joint Resummation for Single-Inclusive Jet Production, Phys. Rev. Lett. **119**, 212001 (2017).

[31] X. Liu, S.-O. Moch, and F. Ringer, Phenomenology of single-inclusive jet production with jet radius and threshold resummation, Phys. Rev. D **97**, 056026 (2018).

[32] J. Currie, E. W. N. Glover, and J. Pires, Next-to-Next-to Leading Order QCD Predictions for Single Jet Inclusive Production at the LHC, Phys. Rev. Lett. **118**, 072002 (2017).

[33] M. Czakon, A. van Hameren, A. Mitov, and R. Poncelet, Single-jet inclusive rates with exact color at $\mathcal{O}(\alpha_s^4)$, J. High Energy Phys. 10 (2019) 262.

[34] G. Arnison *et al.* (UA1 Collaboration), Measurement of the inclusive jet cross section at the CERN *pp* collider, Phys. Lett. B **172**, 461 (1986).

[35] J. Appel *et al.* (UA2 Collaboration), Measurement of the *s* dependence of jet production at the CERN *pp* collider, Phys. Lett. B **160**, 349 (1985).

[36] T. Aaltonen *et al.* (CDF Collaboration), Measurement of the inclusive jet cross section at the Fermilab Tevatron $p\bar{p}$ collider using a cone-based jet algorithm, Phys. Rev. D **78**, 052006 (2008).

[37] V. M. Abazov *et al.* (D0 Collaboration), Measurement of the Inclusive Jet Cross Section in $p\bar{p}$ Collisions at $\sqrt{s} = 1.96$ TeV, Phys. Rev. Lett. **101**, 062001 (2008).

[38] B. Abelev *et al.* (STAR Collaboration), Longitudinal Double-Spin Asymmetry and Cross Section for Inclusive Jet Production in Polarized Proton Collisions at $\sqrt{s} = 200$ GeV, Phys. Rev. Lett. **97**, 252001 (2006).

[39] S. Acharya *et al.* (ALICE Collaboration), Measurement of charged jet cross section in *pp* collisions at $\sqrt{s} = 5.02$ TeV, Phys. Rev. D **100**, 092004 (2019).

[40] B. Abelev *et al.* (ALICE Collaboration), Measurement of the inclusive differential jet cross section in *pp* collisions at $\sqrt{s} = 2.76$ TeV, Phys. Lett. B **722**, 262 (2013).

[41] V. Khachatryan *et al.* (CMS Collaboration), Measurement of the inclusive jet cross section in *pp* collisions at $\sqrt{s_{NN}} = 2.76$ TeV, Eur. Phys. J. C **76**, 265 (2016).

[42] S. Chatrchyan *et al.* (CMS Collaboration), Measurement of the ratio of inclusive jet cross sections using the anti-k_T algorithm with radius parameters $R = 0.5$ and 0.7 in *pp* collisions at $\sqrt{s} = 7$ TeV, Phys. Rev. D **90**, 072006 (2014).

[43] V. Khachatryan *et al.* (CMS Collaboration), Measurement and QCD analysis of double-differential inclusive jet cross sections in *pp* collisions at $\sqrt{s} = 8$ TeV and cross section ratios to 2.76 and 7 TeV, J. High Energy Phys. 03 (2017) 156.

[44] V. Khachatryan *et al.* (CMS Collaboration), Measurement of the double-differential inclusive jet cross section in proton-proton collisions at $\sqrt{s} = 13$ TeV, Eur. Phys. J. C **76**, 451 (2016).

[45] G. Aad *et al.* (ATLAS Collaboration), Measurement of the inclusive jet cross-section in *pp* collisions at $\sqrt{s_{NN}} = 2.76$ TeV and comparison to the inclusive jet cross-section at $\sqrt{s_{NN}} = 7$ TeV using the ATLAS detector, Eur. Phys. J. C **73**, 2509 (2013).

[46] G. Aad *et al.* (ATLAS Collaboration), Measurement of inclusive jet and dijet production in *pp* collisions at $\sqrt{s} = 7$ TeV using the ATLAS detector, Phys. Rev. D **86**, 014022 (2012).

[47] G. Aad *et al.* (ATLAS Collaboration), Measurement of the inclusive jet cross-section in proton-proton collisions at $\sqrt{s} = 7$ TeV using 4.5fb^{-1} of data with the ATLAS detector, J. High Energy Phys. 02 (2015) 153.

[48] D. Britzger, K. Rabbertz, D. Savoiu, G. Sieber, and M. Wobisch, Determination of the strong coupling constant using inclusive jet cross section data from multiple experiments, Eur. Phys. J. C **79**, 68 (2019).

[49] R. D. Ball, S. Carrazza, L. D. Debbio, S. Forte, Z. Kassabov, J. Rojo, E. Slade, and M. Ubiali, Precision determination of

the strong coupling constant within a global PDF analysis, Eur. Phys. J. C **78**, 408 (2018).

[50] B. Malaescu and P. Starovoitov, Evaluation of the strong coupling constant α_S using the ATLAS inclusive jet cross-section data, Eur. Phys. J. C **72**, 2041 (2012).

[51] K. Aamodt *et al.* (ALICE Collaboration), The ALICE experiment at the CERN LHC, J. Instrum. **3**, S08002 (2008).

[52] B. Abelev *et al.* (ALICE Collaboration), Performance of the ALICE Experiment at the CERN LHC, Int. J. Mod. Phys. A **29**, 1430044 (2014).

[53] L. Evans and P. Bryant, The CERN Large Hadron Collider: Accelerator and experiments, J. Instrum. **3**, S08001 (2008).

[54] P. Cortese *et al.* (ALICE Collaboration), ALICE electromagnetic calorimeter technical design report, CERN-ALICE-TDR-014, CERN-LHCC-2008-014, 2008 [http://inspirehep.net/record/794183].

[55] S. Acharya *et al.* (ALICE Collaboration), ALICE 2017 luminosity determination for *pp* collisions at $\sqrt{s} = 5$ TeV, 2018 [http://cds.cern.ch/record/2648933].

[56] B. Abelev *et al.* (ALICE Collaboration), Centrality determination of Pb-Pb collisions at $\sqrt{s_{NN}} = 2.76$ TeV with ALICE, Phys. Rev. C **88**, 044909 (2013).

[57] ALICE Collaboration, Centrality determination in heavy ion collisions [http://cds.cern.ch/record/2636623].

[58] C. Loizides, J. Kamin, and D. d'Enterria, Improved Monte Carlo Glauber predictions at present and future nuclear colliders, Phys. Rev. C **97**, 054910 (2018); Erratum: Improved Monte Carlo Glauber predictions at present and future nuclear colliders [Phys. Rev. C **97**, 054910 (2018)], **99**, 019901(E) (2019).

[59] T. Sjostrand, S. Ask, J. R. Christiansen, R. Corke, N. Desai, P. Ilten, S. Mrenna, S. Prestel, C. O. Rasmussen, and P. Z. Skands, An introduction to PYTHIA 8.2, Comput. Phys. Commun. **191**, 159 (2015).

[60] M. Gyulassy and X.-N. Wang, HIJING 1.0: A Monte Carlo program for parton and particle production in high energy hadronic and nuclear collisions, Comput. Phys. Commun. **83**, 307 (1994).

[61] S. Acharya *et al.* (ALICE Collaboration), π^0 and η meson production in proton-proton collisions at $\sqrt{s_{NN}} = 8$ TeV, Eur. Phys. J. C **78**, 263 (2018).

[62] M. Cacciari, G. Salam, and G. Soyez, The anti-k_T jet cluster algorithm, J. High Energy Phys. 04 (2008) 063.

[63] M. Cacciari, G. Salam, and G. Soyez, The catchment area of jets, J. High Energy Phys. 04 (2008) 005.

[64] B. Abelev *et al.* (ALICE Collaboration), Measurement of event background fluctuations for charged particle jet reconstruction in Pb-Pb collisions at 2.76 TeV, J. High Energy Phys. 03 (2012) 053.

[65] S. Acharya *et al.* (ALICE Collaboration), The ALICE definition of primary particles [https://cds.cern.ch/record/2270008/files/cds.pdf].

[66] A. Hocker and V. Kartvelishvili, SVD approach to data unfolding, Nucl. Instrum. Methods A **372**, 469 (1996).

[67] RooUnfold [http://hepunx.rl.ac.uk/~adye/software/unfold/RooUnfold.html].

[68] G. D'Agostini, A multidimensional unfolding method based on Bayes' theorem, Nucl. Instrum. Methods A **362**, 487 (1995).

[69] S. Alioli, K. Hamilton, P. Nason, C. Oleari, and E. Re, Jet pair production in POWHEG, J. High Energy Phys. 04 (2011) 081.

[70] The POWHEG BOX user manual: Common features [http://th-www.if.uj.edu.pl/~erichter/POWHEG-BOX-V2/Docs/manual-BOX.pdf].

[71] The POWHEG BOX V2 framework [http://th-www.if.uj.edu.pl/~erichter/POWHEG-BOX-V2/Docs/V2-paper.pdf].

[72] ATLAS Collaboration, ATLAS Run 1 PYTHIA8 tunes [https://cds.cern.ch/record/1966419?ln=en].

[73] POWHEG merging [http://home.thep.lu.se/~torbjorn/pythia82html/POWHEGMerging.html].

[74] G. Soyez, A simple description of jet cross-section ratios, Phys. Lett. B **698**, 59 (2011).

[75] Y. He, T. Luo, X.-N. Wang, and Y. Zhu, Linear Boltzmann transport for jet propagation in the quark-gluon plasma: Elastic processes and medium recoil, Phys. Rev. C **91**, 054908 (2015).

[76] A. Idilbi and A. Majumder, Extending soft collinear effective theory to describe hard jets in dense QCD media, Phys. Rev. D **80**, 054022 (2009).

[77] G. Ovanesyan and I. Vitev, An effective theory for jet propagation in dense QCD matter: Jet broadening and medium-induced bremsstrahlung, J. High Energy Phys. 06 (2011) 080.

[78] H. T. Li and I. Vitev, Inverting the mass hierarchy of jet quenching effects with prompt *b*-jet substructure, Phys. Lett. B **793**, 259 (2019).

[79] J. Casalderrey-Solana, D. C. Gulhan, J. G. Milhano, D. Pablos, and K. Rajagopal, A hybrid strong/weak coupling approach to jet quenching, J. High Energy Phys. 10 (2014) 019.

[80] J. Casalderrey-Solana, D. C. Gulhan, J. G. Milhano, D. Pablos, and K. Rajagopal, Predictions for boson-jet observables and fragmentation function ratios from a hybrid strong/weak coupling model for jet quenching, J. High Energy Phys. 03 (2016) 053.

[81] J. Casalderrey-Solana, D. C. Gulhan, J. G. Milhano, D. Pablos, and K. Rajagopal, Angular structure of jet quenching within a hybrid strong/weak coupling model, J. High Energy Phys. 03 (2017) 135.

[82] Z. Hulcher, D. Pablos, and K. Rajagopal, Resolution effects in the hybrid strong/weak coupling model, J. High Energy Phys. 03 (2018) 010.

[83] K. Zapp, F. Krauss, and U. Wiedemann, A perturbative framework for jet quenching, J. High Energy Phys. 03 (2013) 080.

[84] R. Elayavalli and K. Zapp, Simulating V+jet processes in heavy ion collisions with JEWEL, Eur. Phys. J. C **76**, 695 (2016).

[85] J. Putschke *et al.*, The JETSCAPE framework, arXiv:1903.07706.

S. Acharya,[141] D. Adamová,[93] A. Adler,[73] J. Adolfsson,[79] M. M. Aggarwal,[98] G. Aglieri Rinella,[34] M. Agnello,[31] N. Agrawal,[10,53] Z. Ahammed,[141] S. Ahmad,[17] S. U. Ahn,[75] A. Akindinov,[90] M. Al-Turany,[105] S. N. Alam,[141] D. S. D. Albuquerque,[122] D. Aleksandrov,[86] B. Alessandro,[58] H. M. Alfanda,[6] R. Alfaro Molina,[71] B. Ali,[17] Y. Ali,[15] A. Alici,[10,27,53] A. Alkin,[2] J. Alme,[22] T. Alt,[68] L. Altenkamper,[22] I. Altsybeev,[112] M. N. Anaam,[6] C. Andrei,[47] D. Andreou,[34] H. A. Andrews,[109] A. Andronic,[144] M. Angeletti,[34] V. Anguelov,[102] C. Anson,[16] T. Antičić,[106] F. Antinori,[56] P. Antonioli,[53] R. Anwar,[125] N. Apadula,[78] L. Aphecetche,[114] H. Appelshäuser,[68] S. Arcelli,[27] R. Arnaldi,[58] M. Arratia,[78] I. C. Arsene,[21]

M. Arslandok,[102] A. Augustinus,[34] R. Averbeck,[105] S. Aziz,[61] M. D. Azmi,[17] A. Badalà,[55] Y. W. Baek,[40] S. Bagnasco,[58] X. Bai,[105] R. Bailhache,[68] R. Bala,[99] A. Baldisseri,[137] M. Ball,[42] S. Balouza,[103] R. Barbera,[28] L. Barioglio,[26] G. G. Barnaföldi,[145] L. S. Barnby,[92] V. Barret,[134] P. Bartalini,[6] K. Barth,[34] E. Bartsch,[68] F. Baruffaldi,[29] N. Bastid,[134] S. Basu,[143] G. Batigne,[114] B. Batyunya,[74] D. Bauri,[48] J. L. Bazo Alba,[110] I. G. Bearden,[87] C. Bedda,[63] N. K. Behera,[60] I. Belikov,[136] A. D. C. Bell Hechavarria,[144] F. Bellini,[34] R. Bellwied,[125] V. Belyaev,[91] G. Bencedi,[145] S. Beole,[26] A. Bercuci,[47] Y. Berdnikov,[96] D. Berenyi,[145] R. A. Bertens,[130] D. Berzano,[58] M. G. Besoiu,[67] L. Betev,[34] A. Bhasin,[99] I. R. Bhat,[99] M. A. Bhat,[3] H. Bhatt,[48] B. Bhattacharjee,[41] A. Bianchi,[26] L. Bianchi,[26] N. Bianchi,[51] J. Bielčík,[37] J. Bielčíková,[93] A. Bilandzic,[103,117] G. Biro,[145] R. Biswas,[3] S. Biswas,[3] J. T. Blair,[119] D. Blau,[86] C. Blume,[68] G. Boca,[139] F. Bock,[34,94] A. Bogdanov,[91] L. Boldizsár,[145] A. Bolozdynya,[91] M. Bombara,[38] G. Bonomi,[140] H. Borel,[137] A. Borissov,[91,144] H. Bossi,[146] E. Botta,[26] L. Bratrud,[68] P. Braun-Munzinger,[105] M. Bregant,[121] T. A. Broker,[68] M. Broz,[37] E. J. Brucken,[43] E. Bruna,[58] G. E. Bruno,[104] M. D. Buckland,[127] D. Budnikov,[107] H. Buesching,[68] S. Bufalino,[31] O. Bugnon,[114] P. Buhler,[113] P. Buncic,[34] Z. Buthelezi,[72,131] J. B. Butt,[15] J. T. Buxton,[95] S. A. Bysiak,[118] D. Caffarri,[88] A. Caliva,[105] E. Calvo Villar,[110] R. S. Camacho,[44] P. Camerini,[25] A. A. Capon,[113] F. Carnesecchi,[10,27] R. Caron,[137] J. Castillo Castellanos,[137] A. J. Castro,[130] E. A. R. Casula,[54] F. Catalano,[31] C. Ceballos Sanchez,[52] P. Chakraborty,[48] S. Chandra,[141] W. Chang,[6] S. Chapeland,[34] M. Chartier,[127] S. Chattopadhyay,[141] S. Chattopadhyay,[108] A. Chauvin,[24] C. Cheshkov,[135] B. Cheynis,[135] V. Chibante Barroso,[34] D. D. Chinellato,[122] S. Cho,[60] P. Chochula,[34] T. Chowdhury,[134] P. Christakoglou,[88] C. H. Christensen,[87] P. Christiansen,[79] T. Chujo,[133] C. Cicalo,[54] L. Cifarelli,[10,27] F. Cindolo,[53] J. Cleymans,[124] F. Colamaria,[52] D. Colella,[52] A. Collu,[78] M. Colocci,[27] M. Concas,[58,a] G. Conesa Balbastre,[77] Z. Conesa del Valle,[61] G. Contin,[59,127] J. G. Contreras,[37] T. M. Cormier,[94] Y. Corrales Morales,[26,58] P. Cortese,[32] M. R. Cosentino,[123] F. Costa,[34] S. Costanza,[139] P. Crochet,[134] E. Cuautle,[69] P. Cui,[6] L. Cunqueiro,[94] D. Dabrowski,[142] T. Dahms,[103,117] A. Dainese,[56] F. P. A. Damas,[114,137] M. C. Danisch,[102] A. Danu,[67] D. Das,[108] I. Das,[108] P. Das,[84] P. Das,[3] S. Das,[3] A. Dash,[84] S. Dash,[48] A. Dashi,[103] S. De,[84] A. De Caro,[30] G. de Cataldo,[52] C. de Conti,[121] J. de Cuveland,[39] A. De Falco,[24] D. De Gruttola,[10] N. De Marco,[58] S. De Pasquale,[30] S. Deb,[49] B. Debjani,[3] H. F. Degenhardt,[121] K. R. Deja,[142] A. Deloff,[83] S. Delsanto,[26,131] D. Devetak,[105] P. Dhankher,[48] D. Di Bari,[33] A. Di Mauro,[34] R. A. Diaz,[8] T. Dietel,[124] P. Dillenseger,[68] Y. Ding,[6] R. Divià,[34] Ø. Djuvsland,[22] U. Dmitrieva,[62] A. Dobrin,[34,67] B. Dönigus,[68] O. Dordic,[21] A. K. Dubey,[141] A. Dubla,[105] S. Dudi,[98] M. Dukhishyam,[84] P. Dupieux,[134] R. J. Ehlers,[146] V. N. Eikeland,[22] D. Elia,[52] H. Engel,[73] E. Epple,[146] B. Erazmus,[114] F. Erhardt,[97] A. Erokhin,[112] M. R. Ersdal,[22] B. Espagnon,[61] G. Eulisse,[34] D. Evans,[109] S. Evdokimov,[89] L. Fabbietti,[103,117] M. Faggin,[29] J. Faivre,[77] F. Fan,[6] A. Fantoni,[51] M. Fasel,[94] P. Fecchio,[31] A. Feliciello,[58] G. Feofilov,[112] A. Fernández Téllez,[44] A. Ferrero,[137] A. Ferretti,[26] A. Festanti,[34] V. J. G. Feuillard,[102] J. Figiel,[118] S. Filchagin,[107] D. Finogeev,[62] F. M. Fionda,[22] G. Fiorenza,[52] F. Flor,[125] S. Foertsch,[72] P. Foka,[105] S. Fokin,[86] E. Fragiacomo,[59] U. Frankenfeld,[105] U. Fuchs,[34] C. Furget,[77] A. Furs,[62] M. Fusco Girard,[30] J. J. Gaardhøje,[87] M. Gagliardi,[26] A. M. Gago,[110] A. Gal,[136] C. D. Galvan,[120] P. Ganoti,[82] C. Garabatos,[105] E. Garcia-Solis,[11] K. Garg,[28] C. Gargiulo,[34] A. Garibli,[85] K. Garner,[144] P. Gasik,[103,117] E. F. Gauger,[119] M. B. Gay Ducati,[70] M. Germain,[114] J. Ghosh,[108] P. Ghosh,[141] S. K. Ghosh,[3] P. Gianotti,[51] P. Giubellino,[58,105] P. Giubilato,[29] P. Glässel,[102] D. M. Gomez Coral,[71] A. Gomez Ramirez,[73] V. Gonzalez,[105] P. González-Zamora,[44] S. Gorbunov,[39] L. Görlich,[118] S. Gotovac,[35] V. Grabski,[71] L. K. Graczykowski,[142] K. L. Graham,[109] L. Greiner,[78] A. Grelli,[63] C. Grigoras,[34] V. Grigoriev,[91] A. Grigoryan,[1] S. Grigoryan,[74] O. S. Groettvik,[22] F. Grosa,[31] J. F. Grosse-Oetringhaus,[34] R. Grosso,[105] R. Guernane,[77] M. Guittiere,[114] K. Gulbrandsen,[87] T. Gunji,[132] A. Gupta,[99] R. Gupta,[99] I. B. Guzman,[44] R. Haake,[146] M. K. Habib,[105] C. Hadjidakis,[61] H. Hamagaki,[80] G. Hamar,[145] M. Hamid,[6] R. Hannigan,[119] M. R. Haque,[63,84] A. Harlenderova,[105] J. W. Harris,[146] A. Harton,[11] J. A. Hasenbichler,[34] D. Hatzifotiadou,[10,53] P. Hauer,[42] S. Hayashi,[132] S. T. Heckel,[68,103] E. Hellbär,[68] H. Helstrup,[36] A. Herghelegiu,[47] E. G. Hernandez,[44] G. Herrera Corral,[9] F. Herrmann,[144] K. F. Hetland,[36] T. E. Hilden,[43] H. Hillemanns,[34] C. Hills,[127] B. Hippolyte,[136] B. Hohlweger,[103] D. Horak,[37] A. Hornung,[68] S. Hornung,[105] R. Hosokawa,[16,133] P. Hristov,[34] C. Huang,[61] C. Hughes,[130] P. Huhn,[68] T. J. Humanic,[95] H. Hushnud,[108] L. A. Husova,[144] N. Hussain,[41] S. A. Hussain,[15] D. Hutter,[39] J. P. Iddon,[34,127] R. Ilkaev,[107] M. Inaba,[133] G. M. Innocenti,[34] M. Ippolitov,[86] A. Isakov,[93] M. S. Islam,[108] M. Ivanov,[105] V. Ivanov,[96] V. Izucheev,[89] B. Jacak,[78] N. Jacazio,[27,53] P. M. Jacobs,[78] M. B. Jadhav,[48] S. Jadlovska,[116] J. Jadlovsky,[116] S. Jaelani,[63] C. Jahnke,[121] M. J. Jakubowska,[142] M. A. Janik,[142] M. Jercic,[97] O. Jevons,[109] M. Jin,[125] F. Jonas,[94,144] P. G. Jones,[109] J. Jung,[68] M. Jung,[68] A. Jusko,[109] P. Kalinak,[64] A. Kalweit,[34] V. Kaplin,[91] S. Kar,[6] A. Karasu Uysal,[76] O. Karavichev,[62] T. Karavicheva,[62] P. Karczmarczyk,[34] E. Karpechev,[62] U. Kebschull,[73] R. Keidel,[46] M. Keil,[34] B. Ketzer,[42] Z. Khabanova,[88] A. M. Khan,[6] S. Khan,[17] S. A. Khan,[141] A. Khanzadeev,[96] Y. Kharlov,[89] A. Khatun,[17] A. Khuntia,[118] B. Kileng,[36] B. Kim,[60] B. Kim,[133] D. Kim,[147] D. J. Kim,[126] E. J. Kim,[13] H. Kim,[18,147] J. Kim,[147] J. S. Kim,[40] J. Kim,[102] J. Kim,[147] J. Kim,[13] M. Kim,[102] S. Kim,[19] T. Kim,[147] T. Kim,[147] S. Kirsch,[39,68] I. Kisel,[39] S. Kiselev,[90] A. Kisiel,[142] J. L. Klay,[5] C. Klein,[68] J. Klein,[58] S. Klein,[78] C. Klein-Bösing,[144] M. Kleiner,[68] S. Klewin,[102] A. Kluge,[34] M. L. Knichel,[34] A. G. Knospe,[125] C. Kobdaj,[115] M. K. Köhler,[102] T. Kollegger,[105] A. Kondratyev,[74] N. Kondratyeva,[91] E. Kondratyuk,[89] J. Konig,[68] P. J. Konopka,[34] L. Koska,[116] O. Kovalenko,[83] V. Kovalenko,[112] M. Kowalski,[118] I. Králik,[64] A. Kravčáková,[38] L. Kreis,[105] M. Krivda,[64,109] F. Krizek,[93] K. Krizkova Gajdosova,[37] M. Krüger,[68] E. Kryshen,[96] M. Krzewicki,[39] A. M. Kubera,[95] V. Kučera,[60] C. Kuhn,[136] P. G. Kuijer,[88] L. Kumar,[98] S. Kumar,[48] S. Kundu,[84] P. Kurashvili,[83] A. Kurepin,[62] A. B. Kurepin,[62] A. Kuryakin,[107] S. Kushpil,[93] J. Kvapil,[109] M. J. Kweon,[60] J. Y. Kwon,[60] Y. Kwon,[147] S. L. La Pointe,[39] P. La Rocca,[28] Y. S. Lai,[78] R. Langoy,[129] K. Lapidus,[34] A. Lardeux,[21] P. Larionov,[51] E. Laudi,[34] R. Lavicka,[37] T. Lazareva,[112] R. Lea,[25] L. Leardini,[102] J. Lee,[133] S. Lee,[147] F. Lehas,[88] S. Lehner,[113] J. Lehrbach,[39] R. C. Lemmon,[92] I. León Monzón,[120]

E. D. Lesser,[20] M. Lettrich,[34] P. Lévai,[145] X. Li,[12] X. L. Li,[6] J. Lien,[129] R. Lietava,[109] B. Lim,[18] V. Lindenstruth,[39] S. W. Lindsay,[127] C. Lippmann,[105] M. A. Lisa,[95] V. Litichevskyi,[43] A. Liu,[78] S. Liu,[95] W. J. Llope,[143] I. M. Lofnes,[22] V. Loginov,[91] C. Loizides,[94] P. Loncar,[35] X. Lopez,[134] E. López Torres,[8] J. R. Luhder,[144] M. Lunardon,[29] G. Luparello,[59] Y. Ma,[111] A. Maevskaya,[62] M. Mager,[34] S. M. Mahmood,[21] T. Mahmoud,[42] A. Maire,[136] R. D. Majka,[146] M. Malaev,[96] Q. W. Malik,[21] L. Malinina,[74,b] D. Mal'Kevich,[90] P. Malzacher,[105] G. Mandaglio,[55] V. Manko,[86] F. Manso,[134] V. Manzari,[52] Y. Mao,[6] M. Marchisone,[135] J. Mareš,[66] G. V. Margagliotti,[25] A. Margotti,[53] J. Margutti,[63] A. Marín,[105] C. Markert,[119] M. Marquard,[68] N. A. Martin,[102] P. Martinengo,[34] J. L. Martinez,[125] M. I. Martínez,[44] G. Martínez García,[114] M. Martinez Pedreira,[34] S. Masciocchi,[105] M. Masera,[26] A. Masoni,[54] L. Massacrier,[61] E. Masson,[114] A. Mastroserio,[52,138] A. M. Mathis,[103,117] O. Matonoha,[79] P. F. T. Matuoka,[121] A. Matyja,[118] C. Mayer,[118] M. Mazzilli,[33] M. A. Mazzoni,[57] A. F. Mechler,[68] F. Meddi,[23] Y. Melikyan,[62,91] A. Menchaca-Rocha,[71] C. Mengke,[6] E. Meninno,[30,113] M. Meres,[14] S. Mhlanga,[124] Y. Miake,[133] L. Micheletti,[26] D. L. Mihaylov,[103] K. Mikhaylov,[74,90] A. Mischke,[63,c] A. N. Mishra,[69] D. Miśkowiec,[105] A. Modak,[3] N. Mohammadi,[34] A. P. Mohanty,[63] B. Mohanty,[84] M. Mohisin Khan,[17,d] C. Mordasini,[103] D. A. Moreira De Godoy,[144] L. A. P. Moreno,[44] I. Morozov,[62] A. Morsch,[34] T. Mrnjavac,[34] V. Muccifora,[51] E. Mudnic,[35] D. Mühlheim,[144] S. Muhuri,[141] J. D. Mulligan,[78] M. G. Munhoz,[121] K. Münning,[42] R. H. Munzer,[68] H. Murakami,[132] S. Murray,[124] L. Musa,[34] J. Musinsky,[64] C. J. Myers,[125] J. W. Myrcha,[142] B. Naik,[48] R. Nair,[83] B. K. Nandi,[48] R. Nania,[10,53] E. Nappi,[52] M. U. Naru,[15] A. F. Nassirpour,[79] C. Nattrass,[130] R. Nayak,[48] T. K. Nayak,[84] S. Nazarenko,[107] A. Neagu,[21] R. A. Negrao De Oliveira,[68] L. Nellen,[69] S. V. Nesbo,[36] G. Neskovic,[39] D. Nesterov,[112] L. T. Neumann,[142] B. S. Nielsen,[87] S. Nikolaev,[86] S. Nikulin,[86] V. Nikulin,[96] F. Noferini,[10,53] P. Nomokonov,[74] J. Norman,[77] N. Novitzky,[133] P. Nowakowski,[142] A. Nyanin,[86] J. Nystrand,[22] M. Ogino,[80] A. Ohlson,[79,102] J. Oleniacz,[142] A. C. Oliveira Da Silva,[121,130] M. H. Oliver,[146] C. Oppedisano,[58] R. Orava,[43] A. Ortiz Velasquez,[69] A. Oskarsson,[79] J. Otwinowski,[118] K. Oyama,[80] Y. Pachmayer,[102] V. Pacik,[87] D. Pagano,[140] G. Paić,[69] J. Pan,[143] A. K. Pandey,[48] S. Panebianco,[137] P. Pareek,[49,141] J. Park,[60] J. E. Parkkila,[126] S. Parmar,[98] S. P. Pathak,[125] R. N. Patra,[141] B. Paul,[24,58] H. Pei,[6] T. Peitzmann,[63] X. Peng,[6] L. G. Pereira,[70] H. Pereira Da Costa,[137] D. Peresunko,[86] G. M. Perez,[8] E. Perez Lezama,[68] V. Peskov,[68] Y. Pestov,[4] V. Petráček,[37] M. Petrovici,[47] R. P. Pezzi,[70] S. Piano,[59] M. Pikna,[14] P. Pillot,[114] L. O. D. L. Pimentel,[87] O. Pinazza,[34,53] L. Pinsky,[125] C. Pinto,[28] S. Pisano,[10,51] D. Pistone,[55] M. Płoskoń,[78] M. Planinic,[97] F. Pliquett,[68] J. Pluta,[142] S. Pochybova,[145,c] M. G. Poghosyan,[94] B. Polichtchouk,[89] N. Poljak,[97] A. Pop,[47] H. Poppenborg,[144] S. Porteboeuf-Houssais,[134] V. Pozdniakov,[74] S. K. Prasad,[3] R. Preghenella,[53] F. Prino,[58] C. A. Pruneau,[143] I. Pshenichnov,[62] M. Puccio,[26,34] V. Punin,[107] J. Putschke,[143] R. E. Quishpe,[125] S. Ragoni,[109] S. Raha,[3] S. Rajput,[99] J. Rak,[126] A. Rakotozafindrabe,[137] L. Ramello,[32] F. Rami,[136] R. Raniwala,[100] S. Raniwala,[100] S. S. Räsänen,[43] R. Rath,[49] V. Ratza,[42] I. Ravasenga,[31] K. F. Read,[94,130] K. Redlich,[83,e] A. Rehman,[22] P. Reichelt,[68] F. Reidt,[34] X. Ren,[6] R. Renfordt,[68] Z. Rescakova,[38] J.-P. Revol,[10] K. Reygers,[102] V. Riabov,[96] T. Richert,[79,87] M. Richter,[21] P. Riedler,[34] W. Riegler,[34] F. Riggi,[28] C. Ristea,[67] S. P. Rode,[49] M. Rodríguez Cahuantzi,[44] K. Røed,[21] R. Rogalev,[89] E. Rogochaya,[74] D. Rohr,[34] D. Röhrich,[22] P. S. Rokita,[142] F. Ronchetti,[51] E. D. Rosas,[69] K. Roslon,[142] A. Rossi,[29,56] A. Rotondi,[139] F. Roukoutakis,[82] A. Roy,[49] P. Roy,[108] O. V. Rueda,[79] R. Rui,[25] B. Rumyantsev,[74] A. Rustamov,[85] E. Ryabinkin,[86] Y. Ryabov,[96] A. Rybicki,[118] H. Rytkonen,[126] S. Sadhu,[141] S. Sadovsky,[89] K. Šafařík,[34,37] S. K. Saha,[141] B. Sahoo,[48] P. Sahoo,[48,49] R. Sahoo,[49] S. Sahoo,[65] P. K. Sahu,[65] J. Saini,[141] S. Sakai,[133] S. Sambyal,[99] V. Samsonov,[91,96] D. Sarkar,[143] N. Sarkar,[141] P. Sarma,[41] V. M. Sarti,[103] M. H. P. Sas,[63] E. Scapparone,[53] B. Schaefer,[94] J. Schambach,[119] H. S. Scheid,[68] C. Schiaua,[47] R. Schicker,[102] A. Schmah,[102] C. Schmidt,[105] H. R. Schmidt,[101] M. O. Schmidt,[102] M. Schmidt,[101] N. V. Schmidt,[68,94] A. R. Schmier,[130] J. Schukraft,[87] Y. Schutz,[34,136] K. Schwarz,[105] K. Schweda,[105] G. Scioli,[27] E. Scomparin,[58] M. Šefčík,[38] J. E. Seger,[16] Y. Sekiguchi,[132] D. Sekihata,[45,132] I. Selyuzhenkov,[91,105] S. Senyukov,[136] D. Serebryakov,[62] E. Serradilla,[71] A. Sevcenco,[67] A. Shabanov,[62] A. Shabetai,[114] R. Shahoyan,[34] W. Shaikh,[108] A. Shangaraev,[89] A. Sharma,[98] A. Sharma,[99] H. Sharma,[118] M. Sharma,[99] N. Sharma,[98] A. I. Sheikh,[141] K. Shigaki,[45] M. Shimomura,[81] S. Shirinkin,[90] Q. Shou,[111] Y. Sibiriak,[86] S. Siddhanta,[54] T. Siemiarczuk,[83] D. Silvermyr,[79] G. Simatovic,[88] G. Simonetti,[34,103] R. Singh,[84] R. Singh,[99] R. Singh,[49] V. K. Singh,[141] V. Singhal,[141] T. Sinha,[108] B. Sitar,[14] M. Sitta,[32] T. B. Skaali,[21] M. Slupecki,[126] N. Smirnov,[146] R. J. M. Snellings,[63] T. W. Snellman,[43,126] C. Soncco,[110] J. Song,[60,125] A. Songmoolnak,[115] F. Soramel,[29] S. Sorensen,[130] I. Sputowska,[118] J. Stachel,[102] I. Stan,[67] P. Stankus,[94] P. J. Steffanic,[130] E. Stenlund,[79] D. Stocco,[114] M. M. Storetvedt,[36] L. D. Stritto,[30] A. A. P. Suaide,[121] T. Sugitate,[45] C. Suire,[61] M. Suleymanov,[15] M. Suljic,[34] R. Sultanov,[90] M. Šumbera,[93] S. Sumowidagdo,[50] S. Swain,[65] A. Szabo,[14] I. Szarka,[14] U. Tabassam,[15] G. Taillepied,[134] J. Takahashi,[122] G. J. Tambave,[22] S. Tang,[6,134] M. Tarhini,[114] M. G. Tarzila,[47] A. Tauro,[34] G. Tejeda Muñoz,[44] A. Telesca,[34] C. Terrevoli,[125] D. Thakur,[49] S. Thakur,[141] D. Thomas,[119] F. Thoresen,[87] R. Tieulent,[135] A. Tikhonov,[62] A. R. Timmins,[125] A. Toia,[68] N. Topilskaya,[62] M. Toppi,[51] F. Torales-Acosta,[20] S. R. Torres,[9,120] A. Trifiro,[55] S. Tripathy,[49] T. Tripathy,[48] S. Trogolo,[29] G. Trombetta,[33] L. Tropp,[38] V. Trubnikov,[2] W. H. Trzaska,[126] T. P. Trzcinski,[142] B. A. Trzeciak,[63] T. Tsuji,[132] A. Tumkin,[107] R. Turrisi,[56] T. S. Tveter,[21] K. Ullaland,[22] E. N. Umaka,[125] A. Uras,[135] G. L. Usai,[24] A. Utrobicic,[97] M. Vala,[38] N. Valle,[139] S. Vallero,[58] N. van der Kolk,[63] L. V. R. van Doremalen,[63] M. van Leeuwen,[63] P. Vande Vyvre,[34] D. Varga,[145] Z. Varga,[145] M. Varga-Kofarago,[145] A. Vargas,[44] M. Vargyas,[126] M. Vasileiou,[82] A. Vasiliev,[86] O. Vázquez Doce,[103,117] V. Vechernin,[112] A. M. Veen,[63] E. Vercellin,[26] S. Vergara Limón,[44] L. Vermunt,[63] R. Vernet,[7] R. Vértesi,[145] L. Vickovic,[35] J. Viinikainen,[126] Z. Vilakazi,[131] O. Villalobos Baillie,[109] A. Villatoro Tello,[44] G. Vino,[52] A. Vinogradov,[86] T. Virgili,[30] V. Vislavicius,[87] A. Vodopyanov,[74] B. Volkel,[34] M. A. Völkl,[101] K. Voloshin,[90] S. A. Voloshin,[143] G. Volpe,[33] B. von Haller,[34] I. Vorobyev,[103] D. Voscek,[116] J. Vrláková,[38] B. Wagner,[22] M. Weber,[113] S. G. Weber,[105,144]

A. Wegrzynek,[34] D. F. Weiser,[102] S. C. Wenzel,[34] J. P. Wessels,[144] J. Wiechula,[68] J. Wikne,[21] G. Wilk,[83] J. Wilkinson,[10,53] G. A. Willems,[34] E. Willsher,[109] B. Windelband,[102] W. E. Witt,[130] Y. Wu,[128] R. Xu,[6] S. Yalcin,[76] K. Yamakawa,[45] S. Yang,[22] S. Yano,[137] Z. Yin,[6] H. Yokoyama,[63] I.-K. Yoo,[18] J. H. Yoon,[60] S. Yuan,[22] A. Yuncu,[102] V. Yurchenko,[2] V. Zaccolo,[25] A. Zaman,[15] C. Zampolli,[34] H. J. C. Zanoli,[63,121] N. Zardoshti,[34] A. Zarochentsev,[112] P. Závada,[66] N. Zaviyalov,[107] H. Zbroszczyk,[142] M. Zhalov,[96] S. Zhang,[111] X. Zhang,[6] Z. Zhang,[6] V. Zherebchevskii,[112] N. Zhigareva,[90] D. Zhou,[6] Y. Zhou,[87] Z. Zhou,[22] J. Zhu,[6,105] Y. Zhu,[6] A. Zichichi,[10,27] M. B. Zimmermann,[34] G. Zinovjev,[2] and N. Zurlo[140]

(ALICE Collaboration)

[1]*A. I. Alikhanyan National Science Laboratory (Yerevan Physics Institute) Foundation, Yerevan, Armenia*
[2]*Bogolyubov Institute for Theoretical Physics, National Academy of Sciences of Ukraine, Kiev, Ukraine*
[3]*Bose Institute, Department of Physics and Centre for Astroparticle Physics and Space Science (CAPSS), Kolkata, India*
[4]*Budker Institute for Nuclear Physics, Novosibirsk, Russia*
[5]*California Polytechnic State University, San Luis Obispo, California, USA*
[6]*Central China Normal University, Wuhan, China*
[7]*Centre de Calcul de l'IN2P3, Villeurbanne, Lyon, France*
[8]*Centro de Aplicaciones Tecnológicas y Desarrollo Nuclear (CEADEN), Havana, Cuba*
[9]*Centro de Investigación y de Estudios Avanzados (CINVESTAV), Mexico City and Mérida, Mexico*
[10]*Centro Fermi, Museo Storico della Fisica e Centro Studi e Ricerche "Enrico Fermi," Rome, Italy*
[11]*Chicago State University, Chicago, Illinois, USA*
[12]*China Institute of Atomic Energy, Beijing, China*
[13]*Chonbuk National University, Jeonju, Republic of Korea*
[14]*Comenius University Bratislava, Faculty of Mathematics, Physics and Informatics, Bratislava, Slovakia*
[15]*COMSATS University Islamabad, Islamabad, Pakistan*
[16]*Creighton University, Omaha, Nebraska, USA*
[17]*Department of Physics, Aligarh Muslim University, Aligarh, India*
[18]*Department of Physics, Pusan National University, Pusan, Republic of Korea*
[19]*Department of Physics, Sejong University, Seoul, Republic of Korea*
[20]*Department of Physics, University of California, Berkeley, California, USA*
[21]*Department of Physics, University of Oslo, Oslo, Norway*
[22]*Department of Physics and Technology, University of Bergen, Bergen, Norway*
[23]*Dipartimento di Fisica dell'Università 'La Sapienza' and Sezione INFN, Rome, Italy*
[24]*Dipartimento di Fisica dell'Università and Sezione INFN, Cagliari, Italy*
[25]*Dipartimento di Fisica dell'Università and Sezione INFN, Trieste, Italy*
[26]*Dipartimento di Fisica dell'Università and Sezione INFN, Turin, Italy*
[27]*Dipartimento di Fisica e Astronomia dell'Università and Sezione INFN, Bologna, Italy*
[28]*Dipartimento di Fisica e Astronomia dell'Università and Sezione INFN, Catania, Italy*
[29]*Dipartimento di Fisica e Astronomia dell'Università and Sezione INFN, Padova, Italy*
[30]*Dipartimento di Fisica "E. R. Caianiello" dell'Università and Gruppo Collegato INFN, Salerno, Italy*
[31]*Dipartimento DISAT del Politecnico and Sezione INFN, Turin, Italy*
[32]*Dipartimento di Scienze e Innovazione Tecnologica dell'Università del Piemonte Orientale and INFN Sezione di Torino, Alessandria, Italy*
[33]*Dipartimento Interateneo di Fisica "M. Merlin" and Sezione INFN, Bari, Italy*
[34]*European Organization for Nuclear Research (CERN), Geneva, Switzerland*
[35]*Faculty of Electrical Engineering, Mechanical Engineering and Naval Architecture, University of Split, Split, Croatia*
[36]*Faculty of Engineering and Science, Western Norway University of Applied Sciences, Bergen, Norway*
[37]*Faculty of Nuclear Sciences and Physical Engineering, Czech Technical University in Prague, Prague, Czech Republic*
[38]*Faculty of Science, P. J. Šafárik University, Košice, Slovakia*
[39]*Frankfurt Institute for Advanced Studies, Johann Wolfgang Goethe-Universität Frankfurt, Frankfurt, Germany*
[40]*Gangneung-Wonju National University, Gangneung, Republic of Korea*
[41]*Gauhati University, Department of Physics, Guwahati, India*
[42]*Helmholtz-Institut für Strahlen- und Kernphysik, Rheinische Friedrich-Wilhelms-Universität Bonn, Bonn, Germany*
[43]*Helsinki Institute of Physics (HIP), Helsinki, Finland*
[44]*High Energy Physics Group, Universidad Autónoma de Puebla, Puebla, Mexico*
[45]*Hiroshima University, Hiroshima, Japan*
[46]*Hochschule Worms, Zentrum für Technologietransfer und Telekommunikation (ZTT), Worms, Germany*
[47]*Horia Hulubei National Institute of Physics and Nuclear Engineering, Bucharest, Romania*
[48]*Indian Institute of Technology Bombay (IIT), Mumbai, India*
[49]*Indian Institute of Technology Indore, Indore, India*

[50]*Indonesian Institute of Sciences, Jakarta, Indonesia*

[51]*INFN, Laboratori Nazionali di Frascati, Frascati, Italy*

[52]*INFN, Sezione di Bari, Bari, Italy*

[53]*INFN, Sezione di Bologna, Bologna, Italy*

[54]*INFN, Sezione di Cagliari, Cagliari, Italy*

[55]*INFN, Sezione di Catania, Catania, Italy*

[56]*INFN, Sezione di Padova, Padova, Italy*

[57]*INFN, Sezione di Roma, Rome, Italy*

[58]*INFN, Sezione di Torino, Turin, Italy*

[59]*INFN, Sezione di Trieste, Trieste, Italy*

[60]*Inha University, Incheon, Republic of Korea*

[61]*Institut de Physique Nucléaire d'Orsay (IPNO), Institut National de Physique Nucléaire et de Physique des Particules (IN2P3/CNRS), Université de Paris-Sud, Université Paris-Saclay, Orsay, France*

[62]*Institute for Nuclear Research, Academy of Sciences, Moscow, Russia*

[63]*Institute for Subatomic Physics, Utrecht University/Nikhef, Utrecht, Netherlands*

[64]*Institute of Experimental Physics, Slovak Academy of Sciences, Košice, Slovakia*

[65]*Institute of Physics, Homi Bhabha National Institute, Bhubaneswar, India*

[66]*Institute of Physics of the Czech Academy of Sciences, Prague, Czech Republic*

[67]*Institute of Space Science (ISS), Bucharest, Romania*

[68]*Institut für Kernphysik, Johann Wolfgang Goethe-Universität Frankfurt, Frankfurt, Germany*

[69]*Instituto de Ciencias Nucleares, Universidad Nacional Autónoma de México, Mexico City, Mexico*

[70]*Instituto de Física, Universidade Federal do Rio Grande do Sul (UFRGS), Porto Alegre, Brazil*

[71]*Instituto de Física, Universidad Nacional Autónoma de México, Mexico City, Mexico*

[72]*iThemba LABS, National Research Foundation, Somerset West, South Africa*

[73]*Johann-Wolfgang-Goethe Universität Frankfurt Institut für Informatik, Fachbereich Informatik und Mathematik, Frankfurt, Germany*

[74]*Joint Institute for Nuclear Research (JINR), Dubna, Russia*

[75]*Korea Institute of Science and Technology Information, Daejeon, Republic of Korea*

[76]*KTO Karatay University, Konya, Turkey*

[77]*Laboratoire de Physique Subatomique et de Cosmologie, Université Grenoble-Alpes, CNRS-IN2P3, Grenoble, France*

[78]*Lawrence Berkeley National Laboratory, Berkeley, California, USA*

[79]*Lund University Department of Physics, Division of Particle Physics, Lund, Sweden*

[80]*Nagasaki Institute of Applied Science, Nagasaki, Japan*

[81]*Nara Women's University (NWU), Nara, Japan*

[82]*National and Kapodistrian University of Athens, School of Science, Department of Physics, Athens, Greece*

[83]*National Centre for Nuclear Research, Warsaw, Poland*

[84]*National Institute of Science Education and Research, Homi Bhabha National Institute, Jatni, India*

[85]*National Nuclear Research Center, Baku, Azerbaijan*

[86]*National Research Centre Kurchatov Institute, Moscow, Russia*

[87]*Niels Bohr Institute, University of Copenhagen, Copenhagen, Denmark*

[88]*Nikhef, National Institute for Subatomic Physics, Amsterdam, Netherlands*

[89]*NRC Kurchatov Institute IHEP, Protvino, Russia*

[90]*NRC Kurchatov Institute ITEP, Moscow, Russia*

[91]*NRNU Moscow Engineering Physics Institute, Moscow, Russia*

[92]*Nuclear Physics Group, STFC Daresbury Laboratory, Daresbury, United Kingdom*

[93]*Nuclear Physics Institute of the Czech Academy of Sciences, Řež u Prahy, Czech Republic*

[94]*Oak Ridge National Laboratory, Oak Ridge, Tennessee, USA*

[95]*Ohio State University, Columbus, Ohio, USA*

[96]*Petersburg Nuclear Physics Institute, Gatchina, Russia*

[97]*Physics Department, Faculty of Science, University of Zagreb, Zagreb, Croatia*

[98]*Physics Department, Panjab University, Chandigarh, India*

[99]*Physics Department, University of Jammu, Jammu, India*

[100]*Physics Department, University of Rajasthan, Jaipur, India*

[101]*Physikalisches Institut, Eberhard-Karls-Universität Tübingen, Tübingen, Germany*

[102]*Physikalisches Institut, Ruprecht-Karls-Universität Heidelberg, Heidelberg, Germany*

[103]*Physik Department, Technische Universität München, Munich, Germany*

[104]*Politecnico di Bari, Bari, Italy*

[105]*Research Division and ExtreMe Matter Institute EMMI, GSI Helmholtzzentrum für Schwerionenforschung GmbH, Darmstadt, Germany*

[106]*Rudjer Bošković Institute, Zagreb, Croatia*

[107]*Russian Federal Nuclear Center (VNIIEF), Sarov, Russia*

[108] *Saha Institute of Nuclear Physics, Homi Bhabha National Institute, Kolkata, India*
[109] *School of Physics and Astronomy, University of Birmingham, Birmingham, United Kingdom*
[110] *Sección Física, Departamento de Ciencias, Pontificia Universidad Católica del Perú, Lima, Peru*
[111] *Shanghai Institute of Applied Physics, Shanghai, China*
[112] *St. Petersburg State University, St. Petersburg, Russia*
[113] *Stefan Meyer Institut für Subatomare Physik (SMI), Vienna, Austria*
[114] *SUBATECH, IMT Atlantique, Université de Nantes, CNRS-IN2P3, Nantes, France*
[115] *Suranaree University of Technology, Nakhon Ratchasima, Thailand*
[116] *Technical University of Košice, Košice, Slovakia*
[117] *Technische Universität München, Excellence Cluster "Universe," Munich, Germany*
[118] *The Henryk Niewodniczanski Institute of Nuclear Physics, Polish Academy of Sciences, Cracow, Poland*
[119] *The University of Texas at Austin, Austin, Texas, USA*
[120] *Universidad Autónoma de Sinaloa, Culiacán, Mexico*
[121] *Universidade de São Paulo (USP), São Paulo, Brazil*
[122] *Universidade Estadual de Campinas (UNICAMP), Campinas, Brazil*
[123] *Universidade Federal do ABC, Santo Andre, Brazil*
[124] *University of Cape Town, Cape Town, South Africa*
[125] *University of Houston, Houston, Texas, USA*
[126] *University of Jyväskylä, Jyväskylä, Finland*
[127] *University of Liverpool, Liverpool, United Kingdom*
[128] *University of Science and Techonology of China, Hefei, China*
[129] *University of South-Eastern Norway, Tonsberg, Norway*
[130] *University of Tennessee, Knoxville, Tennessee, USA*
[131] *University of the Witwatersrand, Johannesburg, South Africa*
[132] *University of Tokyo, Tokyo, Japan*
[133] *University of Tsukuba, Tsukuba, Japan*
[134] *Université Clermont Auvergne, CNRS/IN2P3, LPC, Clermont-Ferrand, France*
[135] *Université de Lyon, Université Lyon 1, CNRS/IN2P3, IPN-Lyon, Villeurbanne, Lyon, France*
[136] *Université de Strasbourg, CNRS, IPHC UMR 7178, F-67000 Strasbourg, France, Strasbourg, France*
[137] *Université Paris-Saclay Centre d'Etudes de Saclay (CEA), IRFU, Départment de Physique Nucléaire (DPhN), Saclay, France*
[138] *Università degli Studi di Foggia, Foggia, Italy*
[139] *Università degli Studi di Pavia, Pavia, Italy*
[140] *Università di Brescia, Brescia, Italy*
[141] *Variable Energy Cyclotron Centre, Homi Bhabha National Institute, Kolkata, India*
[142] *Warsaw University of Technology, Warsaw, Poland*
[143] *Wayne State University, Detroit, Michigan, USA*
[144] *Westfälische Wilhelms-Universität Münster, Institut für Kernphysik, Münster, Germany*
[145] *Wigner Research Centre for Physics, Budapest, Hungary*
[146] *Yale University, New Haven, Connecticut, USA*
[147] *Yonsei University, Seoul, Republic of Korea*

[a]Present address: Dipartimento DET del Politecnico di Torino, Turin, Italy.
[b]Present address: M. V. Lomonosov Moscow State University, D. V. Skobeltsyn Institute of Nuclear, Physics, Moscow, Russia.
[c]Deceased.
[d]Present address: Department of Applied Physics, Aligarh Muslim University, Aligarh, India.
[e]Present address: Institute of Theoretical Physics, University of Wroclaw, Poland.